Effects of Power System Harmonics on Distribution Transformer Insulation Performance

by

Muhammad Hamid

A thesis
presented to the University of Waterloo
in fulfillment of the
thesis requirement for the degree of
Master of Applied Science
in
Electrical and Computer Engineering

Waterloo, Ontario, Canada, 2011

I hereby declare that I am the sole author of this thesis. This is a true copy of the thesis, including any required final revisions, as accepted by my examiners.

I understand that my thesis may be made electronically available to the public.

Abstract

Floating feeder resonances are one of the new challenges being put forward by the renewable energy based distributed generation (DG) installations. Generally, the harmonic injection from DGs are within IEEE standard 519-1992 limits. Although the harmonics are within the IEEE limits, they are a potential threat to power equipment's insulation system integrity due to floating feeder resonances. There is a reasonable probability that at some point in time the feeder resonant frequency may coincide with one of the injected harmonics. Such phenomenon amplifies the specific harmonic causing additional stress on the equipment's insulation system.

In this thesis a feeder resonance study is done on the IEEE 34 bus distribution feeder to show the resonance shift problem in a DG loaded distribution feeder. Electric field study is then carried out on transformer winding to assess the dependence of electric field on harmonic distortion. At first the acoustic emission (AE) technique is employed to identify the change in the electric field distribution inside the winding at higher frequency. The AE technique together with the acoustic waveguide is utilized to locate the partial discharges under power frequency and high frequency operation. The results show a change in partial discharge (PD) location, which implies that the electric field redistributes in the transformer winding at higher frequency In order to further understand the electric field distribution, a high voltage air core coil is modeled by R, L and C ladder network. The R, L and C parameters are solved by finite element method and finally the electric field is calculated by computing the node potentials in the ladder network at various frequencies. The electric field results show that at high frequency distortion the electric stress enhances between fourth and fifth layer of the winding which may give rise to a PD activity; hence degrading the insulation.

An aging experiment is also performed to understand the impact of high frequency distortion on transformer paper insulation. Paper samples are taken from a field aged transformer. They are aged for 72 hours under power frequency and various distorted waveforms. Dissipation factor is used as a comparison tool for paper samples before and after aging. Results show that paper samples aged under distorted waveforms showed a double increase in dissipation factor compared to the samples aged under power frequency.

Acknowledgements

I am greatly in debt to my supervisor Dr. Shesha Jayaram for all her help, support, and guidance throughout the duration of my program. Thank you Doctor.

I would like to thank my readers Dr. Kankar Bhattacharya and Dr. Jatin Nathwani for their valuable comments towards my work and Mrs. Kathy Holston for taking the burdensome job of proof reading.

Thanks are due to Dr. Ayman-El-Hag and Dr. Emad Sharifi for sharing their knowledge and providing guidance during my time at HVEL. I thank Mr. Michael for his technical help during my work at HVEL. I would also like to thank other members of HVEL, including Saleh, Susan, Chitral, Suat, and Paria for their company.

My special thanks go to Ahmed, Refat and Utkarsh for a wonderful time we shared together.

I am also grateful to Dr. Kankar Bhattacharya for giving me access to PSCAD/EMTDC™ license and NSERC, Moloney Electric Inc., Waterloo Institute of Sustainable Energy (WISE) and Hydro One for providing material and financial support to my study.

Finally, I cannot thank enough to my Amma (mother) for everything she has done for me so I can achieve things I never thought I could, my uncle Dr. Arif Khan for his support to my family in difficult times, without which I will not be able to continue my studies, and my brothers Bilal and Hasan and sister Amna for their love and never ending encouragement.

Dedication

This is dedicated to my late father Hamid Wahab and all the people who martyred in the Tunisian, Egyptian, Libyan and Syrian uprising.

Contents

List of Tables

List of Figures

Chapter 1

Introduction

The distribution network of today is much more different than it was a few years ago. With an increased concern about the greenhouse gas emission from conventional coal based power sources and concurrent improvement in semiconductor technology the focus is shifting towards environmentally friendly sources of energy. Therefore, a significant penetration of renewable energy sources is anticipated in the transmission and distribution (T&D) network.

Ontario has already passed a green energy act (GEA) and it is planning to shut down its coal based generation by 2014. Also, some of the nuclear plants are going for refurbishment which will create a net energy deficit. Electric utilities are planning to make up the deficit by implementing efficient energy management plans, adding more renewable sources, particularly wind and solar, and increasing gas based generation. It will certainly improve the renewable portfolio of the province.

In addition, smart grid plans are also in progress. Although there is no specific definition of smart grid, some institutions such as the US Department of Energy (DOE) has defined some basic requirements of a smart grid which are listed in citation [1]. These requirements directly favour connection of distributed generators (DG) in the transmission and distribution network, consequently increasing the wind and solar power penetration in the network.

Most of the DGs such as wind farms, photovoltaic solar power plants and fuel cells connect to grid through power converter based interface. Earlier, line commutated switch-

ing schemes were used in power converters; resulting in single switching per cycle.But due to rapid progression in semiconductor technology, nowadays, insulated gate bipolar transistors (IGBT) are used, which are capable of switching tens of thousands of times per cycle.

Such fast switching characteristics help implement better converter control schemes. But at the same time it has made DGs a potential source of harmonic distortion. The harmonics emission limits identified by power quality standards such as IEEE 519 and IEC 61000-2-2 can be violated because of harmonics amplification induced by feeder resonance [2]. Distribution feeders with multiple wind farms are most susceptible to harmonic limits violation. The high frequency components injected as a consequence of feeder resonance are expected to stress the insulation system of critical power system components like substation transformers and underground cables.

1.1 Distributed Generation

Power system evolution spans over a century and a half. The first commercial power station commenced its operation in 1882. From then to 1935 the power sector was almost a monopoly of big investors. Until 1929, almost 80% of US utilities were owned by 16 companies. The great depression of 1930 forced the federal government to get involved in the power sector. This led to opening up the power sector and approval of some important legislations from the Senate such as the Public Utilities Holding Company Act of 1935 (PUHCA). This law actually restructured the energy sector and limited the operations of utilities to a single state [3]. The post-depression era saw a rapid growth of the power sector. Several rural electrification programs and hydro projects were initiated as a consequence of the Federal Power Act of 1935 (FPA) [4]. Electricity markets began to flourish with inter-state grid connections.

With the expansion of the electricity market and fast paced industrial growth, environmental concerns started to develop which led to the establishment of the US Environmental Protection Agency (EPA) in 1970 [5]. The Public Utilities Regulatory Policy Act (PURPA) of 1978 was the first step towards the de-regulation of the monopolistic electricity market [6]. It forced the power companies to purchase the power from more efficient producers

if the cost was less than their avoided cost. Although the intention behind this legislation was to promote the renewable power resources because of the Arab oil embargo of 1973, it somehow failed to achieve this goal. After the Arab oil embargo when oil prices became sky high, US Congress took initiative for energy conservation, energy efficiency and renewable resources of energy. Because of the embargo, the US government passed much legislation demanding from power producers energy efficiency and alternative methods of power production. The Energy Policy Act of 1992 [7] is one of such piece of legislation which promoted energy efficiency and supported deregulated natural gas production as co-generation. It also introduced a new entity called Independent Power Producers (IPP). After PURPA of 1978 it is the second major legislation which further opened up the grid for dispersed generators. The Federal Energy Regulatory Commission (FERC) Order No. 888 and Order No. 2000 [8, 9] further facilitated the IPPs to hook up their generators on the transmission and distribution network by assigning a third party independent system operator (ISO) to manage the grid activities which was earlier handled by the utilities. Also it required the transmission and distribution network owners to set non-discriminatory tariffs for all generators.

Besides the government initiatives to encourage distributed generation (DG) and reduced greenhouse gas (GHG) emission benefits, there are some system level advantages which motivate utilities to encourage DG connections on their network. DG deferred the requirement to build a new T&D network, and the lead time for DGs is much less compared to conventional centrally planned resources. If correctly planned DGs can also improve the feeder's voltage profile. Since they are installed near to the load they also reduce the T&D congestion and hence reduce the T&D operational cost.

The economics of conventional generation are still better than renewable based generation, but due to the aforementioned advantages, renewable sources make up an appreciable portion of Canada's distributed generation. It is mainly due to the renewable portfolio standard (RPS) which requires the utilities to generate at least some portion of their total production from renewable sources other than hydro [10]. Also some favourable government policies like the Feed In Tariff program (FIT) [11] which was introduced in the Green Energy Act of 2009 [12] encouraged the investors to invest in green energy.

Although much has been done to deregulate the power system to promote the distributed generation, still there is no mutual consensus on the definition of distributed

generation (DG) resources. People have generally defined DG based on following criteria:

a. Voltage level

b. Unit connection

c. Type of prime mover e.g. renewable or co-generation

d. Generation not being dispatched

e. Maximum power rating

For example the International Council on Large Electricity System (CIGRE WG 37-23) defines distributed generation as a unit which is [13, 14, 15]

a. Not centrally planned

b. Today not centrally dispatched

c. Usually connected to the distributed network

d. Smaller than 50-100 MW.

On contrary IEEE defines DG as *"the generation of electricity by facilities that are sufficiently smaller than central generating plants so as to allow interconnection at nearly any point in a power system"* [13, 15, 16, 17].

The International Energy Agency (IEA) defines distributed generation as *"units producing power on a customers' site or within local distribution utilities, and supplying power directly to the local distribution network."* [16]

The California Public Utility Commission (CPUC) defines distributed generation as *"small scale electric generating technologies installed at, or in close proximity to, the end-user's location which can be installed on the end-user side of the meter, or on the grid side."* [18].

If the aforementioned definitions are considered, then they cover a broad range of energy sources which fall under the category of dispersed generation. Having identified this problem, Ackermann et al. [19] have done a thorough literature survey on the definition of DGs. He defines dispersed generation as *"an electric power source connected directly to the distribution network or on the customer site of the meter."*

1.2 Characteristics of Distributed Generators

Distributed generators are classified based on their production level and type of energy resource. As per production level there are four categories [20].

1. Micro DG < 5 kW
2. Small DG 5 kW–5 MW
3. Medium DG 5 MW–50 MW
4. Large DG 50 MW–300 MW

From the point of view of energy sources DGs are mainly classified as [20]

1. Renewables
2. Non-renewables

Renewable energy based distributed generators (REDG) mainly use power converter based interface to connect to the grid. However, non-renewables use synchronous generator based interface with the grid. Synchronous generators have long been used in the power system as the prime machine for energy conversion. It is exceptional in terms of power quality.

As discussed earlier in Section 1.1, due to environmental concerns and simultaneous improvement in technology together with re-assuring government policies for renewable energy sources, wind and solar power are becoming an appreciable portion of Canada's energy mix.

1.3 Ontario's Supply Mix—A Review

Before 2006 Ontario's energy mix was mainly composed of hydro, coal and nuclear based generation. Coal generation made up around 21% of the total power production in 2006 where as renewable energy based generation, excluding hydro, only made up 1.5% of total

generation as shown in Fig 1.1. The province has now set goals to completely shut down coal generation by 2014. In a drive to eradicate the the coal fired power plants, Government of Ontario has successfully managed to reduce the coal based generation by 70% since 2003 [21] and renewable energy profile is also improved from 1.5% to 4.2% as shown in Fig 1.1. It will certainly create the energy gap which needs to be filled by alternative energy production. The energy deficit will be further exacerbated by the refurbishment of most of the nuclear plants. Ontario Power Authority (OPA) has devised a plan to make up this deficit by Demand Side Management (DSM) plans and more wind and solar generation [21]. Additionally, Ontario has invested a substantial amount in wind and solar based

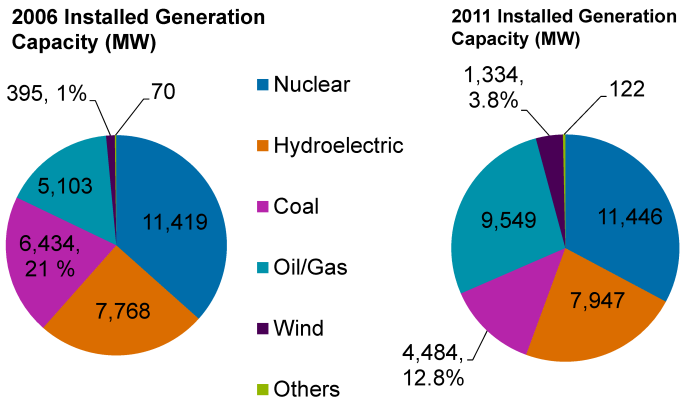

Figure 1.1: Ontario's supply mix in 2006 and 2011 respectively [22, 23]

generation and has become the leader among all other Canadian provinces. It has now the world's largest photovoltaic power plant which was commissioned recently in 2010 and has the total installed capacity of 80 MW [24]. Also, Ontario has the largest wind farm in Canada near Shelburne with a total installed capacity of 199.5 MW [21].

Ontario is not alone however in taking green energy initiatives. If we look at the global statistics from 2003 onwards there is a general inclining trend of green energy based generation as shown in Fig 1.2–Fig 1.5 [25] It is projected that Ontario's population will grow 25% by 2025. This growth would be in the urban population. Around 38% population growth is projected in the greater Toronto area (GTA). There will also be growth in the industrial sector over the years and we will see more electric cars on road. Currently, Ontario's total installed capacity is approximately 35,000 MW. But around 15,000 MW

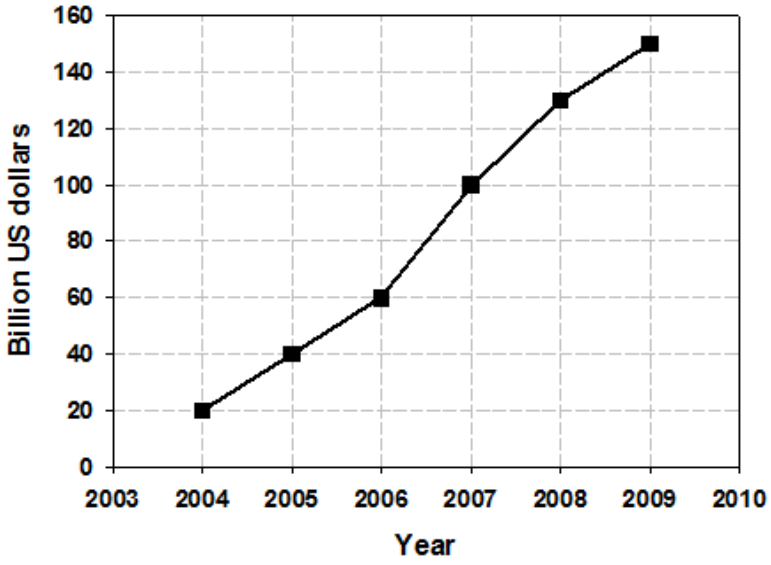

Figure 1.2: Global investments in renewable energy from 2004 to 2009 [25]

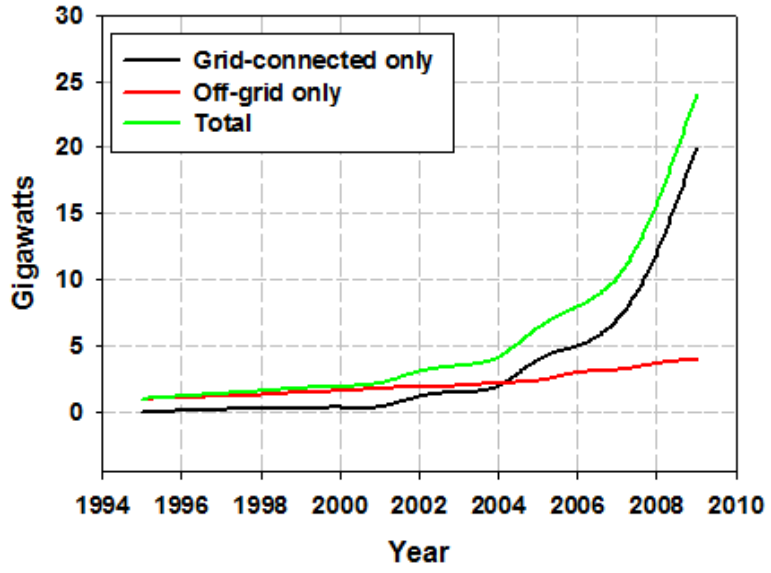

Figure 1.3: Global photovoltaic capacity from 1995 to 2009 [25]

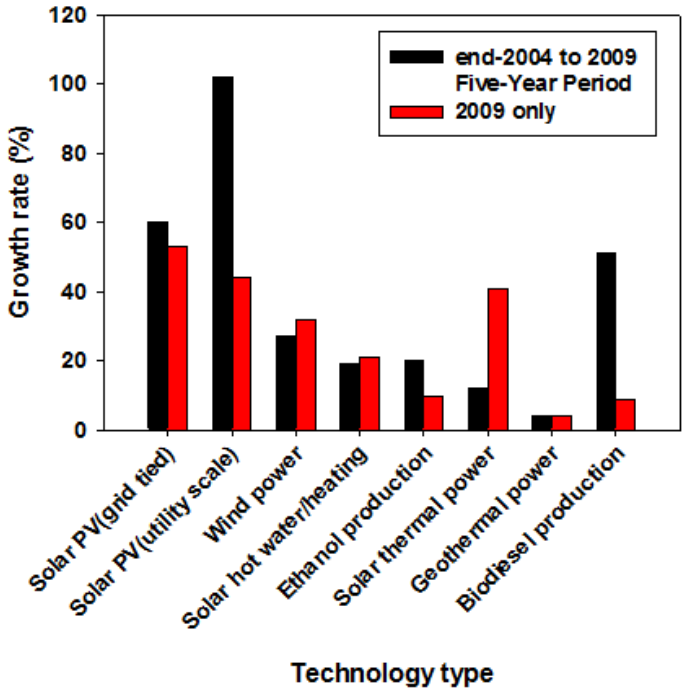

Figure 1.4: Average annual growth rate of renewable energy [25]

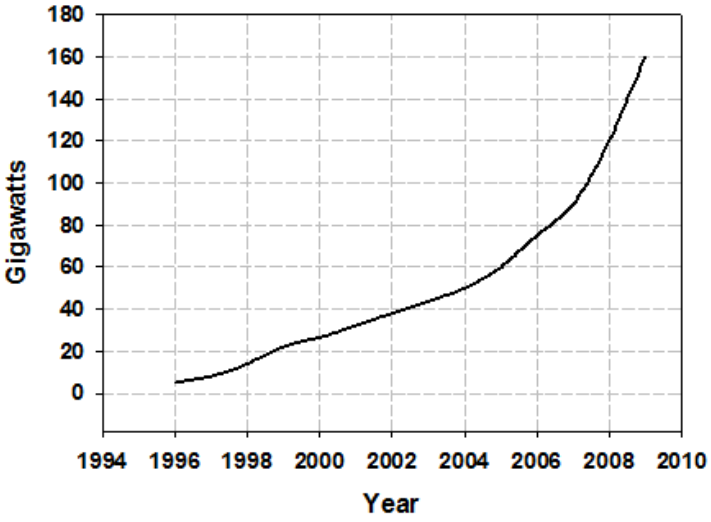

Figure 1.5: Global wind power capacity from 1996 to 2009 [25]

of power will either be retired or needs refurbishment in the coming years. Therefore, the biggest challenge for the province is to plan for not only the demand growth but also for the power plants retirement and refurbishments. Ontario Power Authority (OPA) is responsible for planning and forecasting demand for the province. As per their plan, the province is targeting 10,700 MW of renewable power, excluding the hydro-electric power [21]. This is indeed an appreciable amount of power solely coming from non-hydro renewable resources. However, in order to tap these resources it has been identified that there is a need to expand the T&D network. Therefore the province has invested approximately $7.5 billion for the network expansion [21].

1.4 Wind Power Generation

Ever since wind power generation was proposed it has been evolving every day. At present there are many designs available in the market which differ from each other on many factors like fixed speed or variable speed operation, type of connection with the turbine and type of interface with the grid.

Based on the type of generators used, wind generators can be broadly classified as induction generators (IG), doubly fed induction generators (DFIG), field excited synchronous generators (FESG) and permanent magnet synchronous generators (PMSG) [26, 27].

Another way to classify wind generators is by the type of their connection with the turbine—gear or direct connected. Up to late 90's the manufacturers preferred gear connected over the direct connected, the reason being that they are light in weight because they convert relatively low wind speed to a high rotational speed required by the induction generators. Because of this ability the size of an induction generator was very small; thus the total weight of the system is much less compared to direct drive system [27]. However, the main disadvantage of such an approach is the drastically reduced efficiency of the system [28]. Due to this reason the manufacturers are now more interested in direct drive generators. Currently, only synchronous generators are available in this type. Table1.1 shows the comparison of the latest available wind generators [27]. It is obvious that direct drive generators are heavier than gear connected. Also, Ponder et al [26] have mentioned that direct driven types are even more expensive than gear driven, but still the focus is

Table 1.1: Some of the latest wind generators [27]

No.	Generator type	Gearbox	Manufacture	Power Rating	Turbine Rotor Speed Range	Generator Voltage Rating	Grid Connection Type	Nacelle Weight	Generator Weight
1	FESG	Yes	DeWind	2 MW	11.1 - 20.7 rpm	13.8 KV	4	62,000 kg	N/A
2	FESG	direct drive	Enercon	4.5 MW	N/A	N/A	2	N/A	220,000 kg
3	IG	Yes	Vestas	850 kW	26 rpm	690 V	2	38,000 kg	N/A
4	IG	Yes	Vestas	2 MW	16.7 rpm	690 V	2	67,000 kg	N/A
5	IG	Yes	Vestas	3 MW	N/A	1000 V	3	70,000 kg	N/A
6	DFIG	Yes	Gamesa	850 kW	16.2 - 30.8 rpm	690 V	3	33,000 kg	N/A
7	DFIG	Yes	DeWind	2 MW	11.1 - 2.7 rpm	690 V	3	62,000 kg	N/A
8	DFIG	Yes	Gamesa	2 MW	9 -19 rpm	690 V	4	107,000 kg	N/A
9	PMSG	direct drive	Zephyros	1.5 MW	18 rpm	3000 V	4	N/A	47,200 kg
10	PMSG	direct drive	Vestas	3 MW	N/A	N/A	4	70,000 kg	N/A
11	PMSG	direct drive	The Switch	3.8 MW	21 rpm	690 V	4	N/A	81,000 kg
12	PMSG	Yes	The Switch	950 kW	N/A	690 V	4	N/A	3,400 kg

shifting towards the direct drive generator because of their higher efficiency. Based on the type of grid interconnection there are four classifications of wind generators— Type I to Type IV. Type I and II are directly connected to the grid and both of them use induction generators. The only difference is that Type II has a wound rotor which is connected to an external resistance through slip rings in order to control the slip of the machine to make better use of the available wind speed. They are induction machines and require excitation from an external source; therefore they are available in small sizes up to 500 kVA [29]. The schematic representation of Type I and II wind generators is shown Fig 1.6 and Fig 1.7 respectively [29]. Type III is more popularly known as Doubly Fed Induction Generator (DFIG). The schematic representation of DFIG is shown in Fig 1.8. In this type both rotor and stator are connected to the grid. However, the stator is connected directly, whereas the rotor is connected through two back-to-back power converters. The grid side converter allows the machine to operate in both sub-synchronous and super-synchronous mode. The rotor side converter allows the independent control of machine's torque and speed through vector control technique [29, 30]. The advantage of DFIGs over Type I and Type II is that they make full use of the available wind power by adjusting the rotor speed

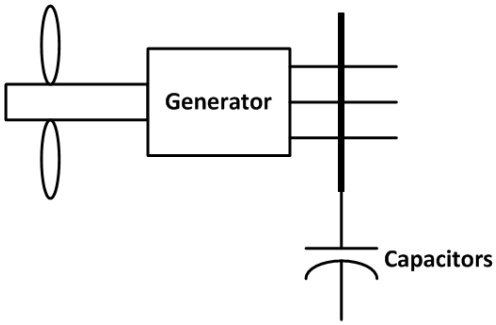

Figure 1.6: Schematic representation of Type-I wind generator [27]

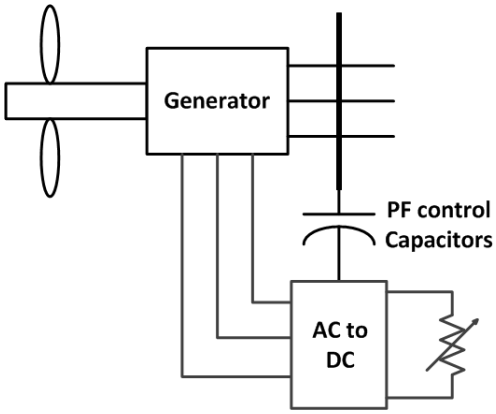

Figure 1.7: Schematic representation of Type-II wind generator [27]

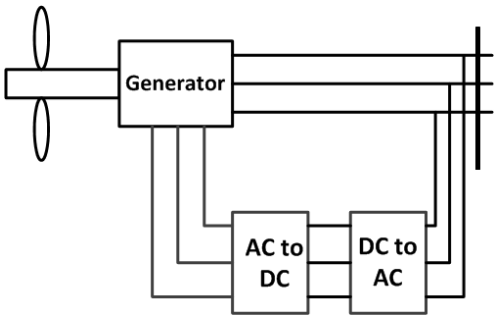

Figure 1.8: Schematic representation of Type-III wind generator [27]

to maintain a constant power coefficient, C_p. Also the converter is rated only 30 percent of the generator rated power to handle the slip power. So the cost of converter is quite low compared to a full rated converter used in Type IV [27]. Type IV generators are mostly direct drive synchronous generators. They are connected to the grid through a full rated power electronic converter as shown in Fig 1.9 [27]. Because they are connected through

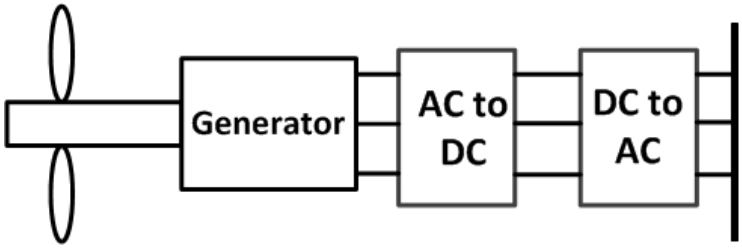

Figure 1.9: Schematic representation of type-IV wind generator [27]

a converter, there is no need to design a high pole machine to accommodate the lower turbine speed. Usually Type IV generators have fewer poles and they produce power at 16 to 20 Hz, which is converted to DC and then converted back to AC at a desired frequency. This approach makes them very versatile. They can get the maximum out of the available wind power at any wind speed [27].

Type I and II are mainly fixed speed wind generators. They are cheaper compared to Types III and IV. According to Burton, et al.[31], generally the wind speed distribution is a Weibull distribution defined by (1.1) with different shape factors, k depending on the site as shown in Fig 1.10. Fixed speed generators are installed on those sites where the k factor has a high value, usually greater than 2. On the contrary the variable speed generators are installed on sites with flatter wind distribution.

$$h(V_o) = (\frac{k}{l})(\frac{V_o}{l})^{k-l} e^{(-\frac{V_o}{l})^k} \qquad for \quad 0 < V_o < \infty \tag{1.1}$$

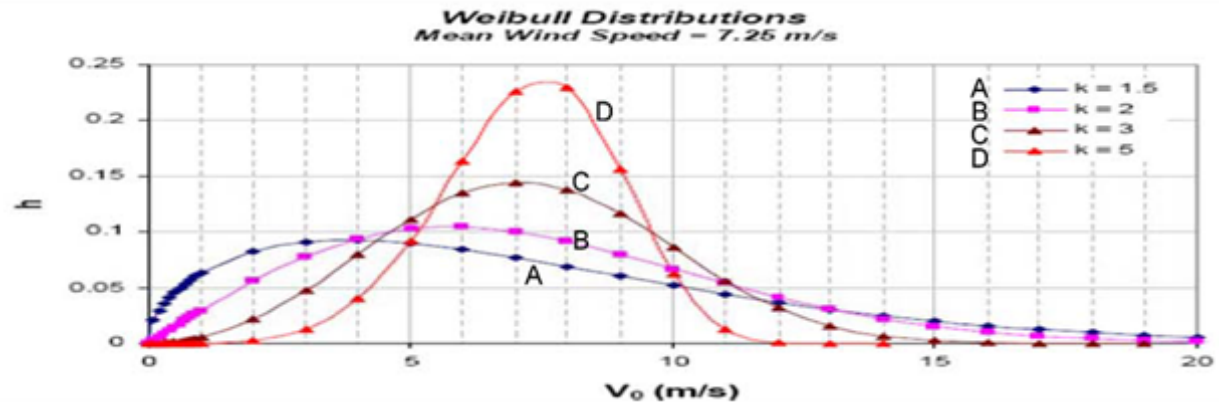

Figure 1.10: Weibull distributions of wind speeds[31]

1.5 Solar Power Generation

Solar technology developed aggressively in the decade of 70's when oil prices became sky high due to the 1973 Arab oil embargo. Governments at that time invested significantly in the research and development (R&D) of solar technology. Consequently, there was a drastic reduction in the per unit price of photovoltaic production from one hundred U.S. dollars per Watt ($100/Watt) in 1971 to seven U.S. dollars per Watt ($7/Watt) in 1985 [32]. However, when world oil prices started to settle down, the government funding got reduced and little progress was seen from 1983 through 1994.

Once again the post 1994 era saw a rapid growth in solar technology, this time primarily due to environmental concerns. Governments took initiatives like feed-in-tariff (FIT) programs to make the economics of solar energy comparable to the conventional sources. Because of this reason there was a substantial increase in the installed solar capacity in some European and North American countries. For instance, Germany's total installed capacity increased from 100 MW to approximately to 4,150 MW because of a FIT program [33]. Also, in 2010 Canada commissioned the world's largest photovoltaic power plant in Sarnia with a total installed capacity of approximately 80 MW [24].

Following are the two main types of solar technologies [34, 35]:

1. Solar thermal power plants more popularly known as concentrated solar power (CSP)

2. Solar Photovoltaic (SPV).

The basic difference in the two is their method of energy conversion. Solar thermal power plants are like any other fossil fuel power plant. Instead of coal or furnace oil, solar energy is utilized to make super heated steam. There are many variants of CSP technology as shown in Table 1.2 [35]. Figure 1.11 and Fig 1.12 show parabolic trough and linear Fresnel

Table 1.2: Variants of CSP technology [35]

Optical method		Focus	Temperture (°C)	Heat transport to boiler
1	Parabolic trough mirror	Line moving	300 - 550	Oil, liquid salt, water + steam
2	Linear Fresnel	Line stationary	250 - 500	Water + steam
3	Linear Fresnel lens	Line moving	250 - 400	N/A
4	Solar tower with field of heliostats	Point Stationary	300 - 1000	Air, liquid salt water + steam gas turbine
5	Solar dish	Point moving	400 - 1500	Stirling engine
6	Fresnel lens (c)	Point moving	400 - 1200	Micro turbine

mirror technology. Both of them are based on line focus of a solar beam. A glass tube containing therminol or molten salt is placed on the line focus to carry the solar heat which is then exchanged in a heat exchanger to generate the super heated steam [35]. In contrast to the first two types in Table 1.2, the other three types are based on point focus. All the mirrors can be rotated on two axes. The beam is focused on a single point; therefore, higher temperatures are possible in this technology. Figure 1.13 shows the concentrated solar tower type where all the beams are focused on a single point on the top of tower.

Solar photovoltaic is another type of solar power conversion. Solar photovoltaic directly converts the solar energy into electrical energy using the photo voltaic effect. SPV systems are either installed as a standalone system with some storage capacity or as a hybrid system with some other form of generation, usually fossil fuel, to complement the power generation

Figure 1.11: Parabolic trough technology

Figure 1.12: Linear Fresnel technology

during shade time [36]. They are also installed in a grid connected mode as shown in Fig 1.14 [37]. The most fundamental component of a SPV system is the solar cell as shown in Fig1.15 [38]. A solar cell consists of a p-n junction in which charges are separated at the junction creating a field inside the cell. When light is cast on the cell it produces free charges which are separated by the field. Hence a voltage is built up across the cell. A

Figure 1.13: Concentrated Solar technology

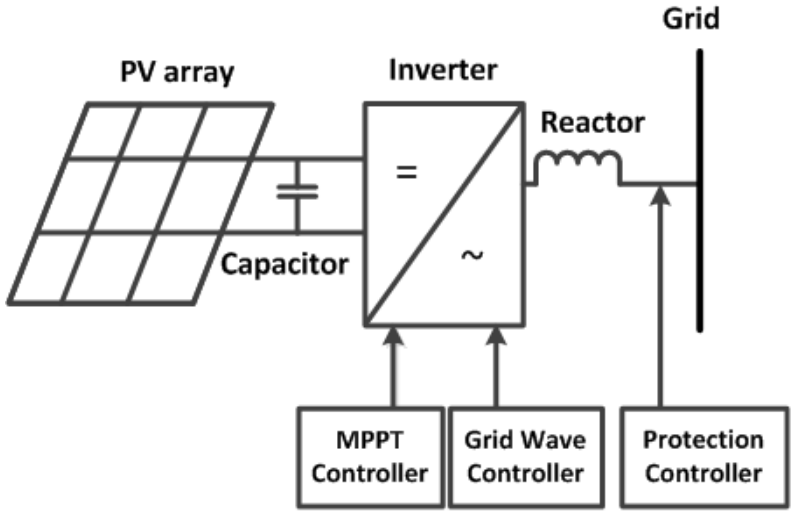

Figure 1.14: Schematic representation of Grid connected Solar Photovoltaic power plant

current flows if the load is connected across the solar cell. A single solar cell can generate only small voltages between 0.6-0.7 V. Therefore they are connected in series to make a solar module. Similarly, the modules are connected together to make a panel, and panels are connected in an array to make up the entire SPV system. Commercially, SPV cells are

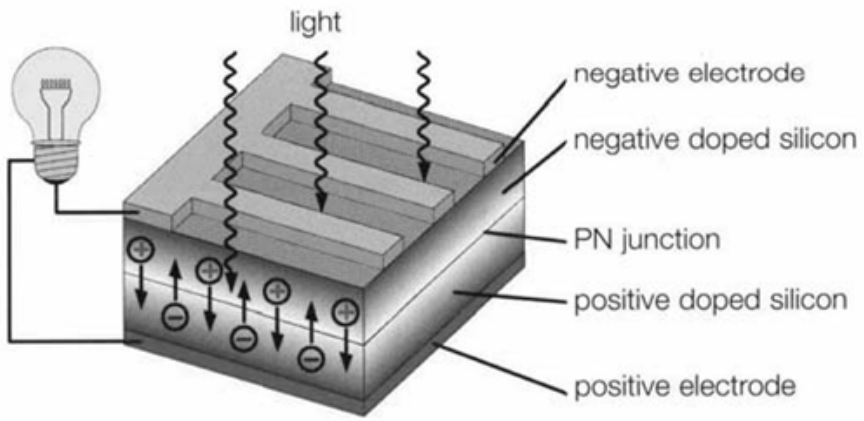

Figure 1.15: Schematic representation of a fundamental solar cell [38]

available in mono crystalline, polycrystalline or amorphous materials both as wafers and thin films.

Usually standalone SPV systems are used in remote areas with no or very limited amount of electrical generation. Sometimes when rural areas have a diesel generator, SPV standalone systems are economical to operate as a hybrid system. When SPV systems are installed as standalone systems they also use batteries in parallel to store the additional energy to be utilised later. However, when SPV systems, whether rooftops or large solar farms, are connected to the grid they are directly interfaced through a power converter. The inverters are used because the SPV system generates DC current which needs to be converted back to AC to drive the AC loads. There are many variants of grid connected SPV available. However the difference lies in the types of solar cells and the type of control strategy used for the inverter.

The power level of SPV systems depends on both cell temperature and the insolation level as shown in Fig 1.16 and Fig 1.17 [37]. In order to get the maximum efficiency out of the SPV systems, they are equipped with maximum power point tracking (MPPT) controllers. However, there are many MPPT controlling techniques proposed in the literature [39, 40, 41].

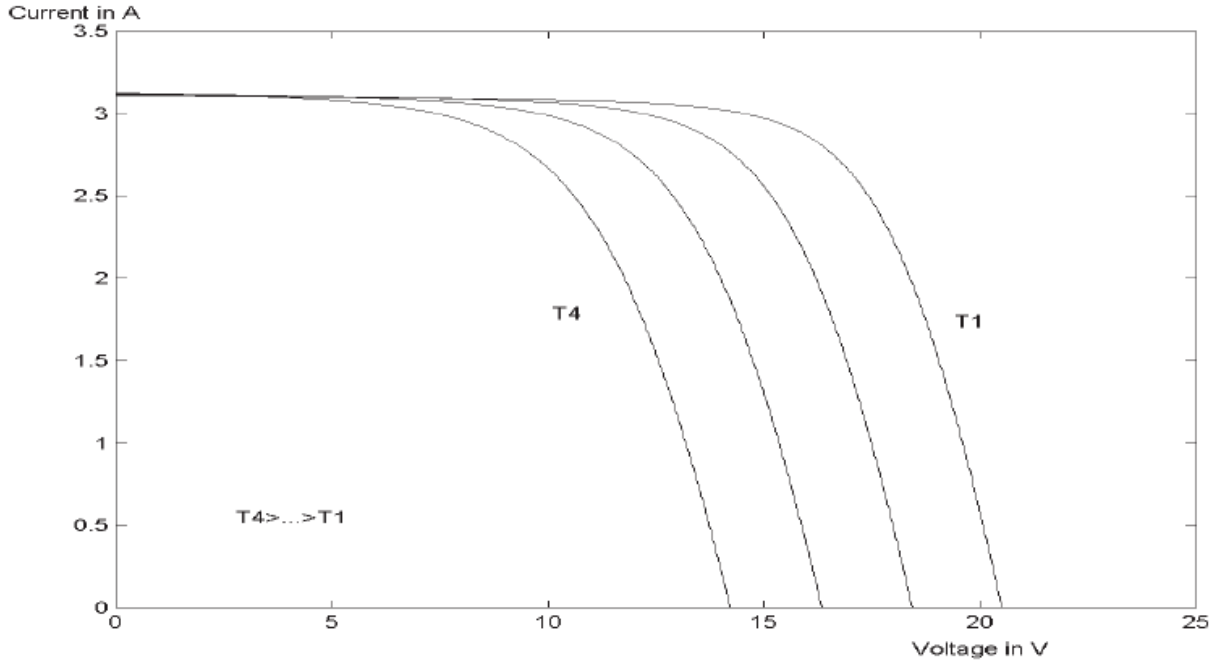

Figure 1.16: Effect of temperature on output current [37]

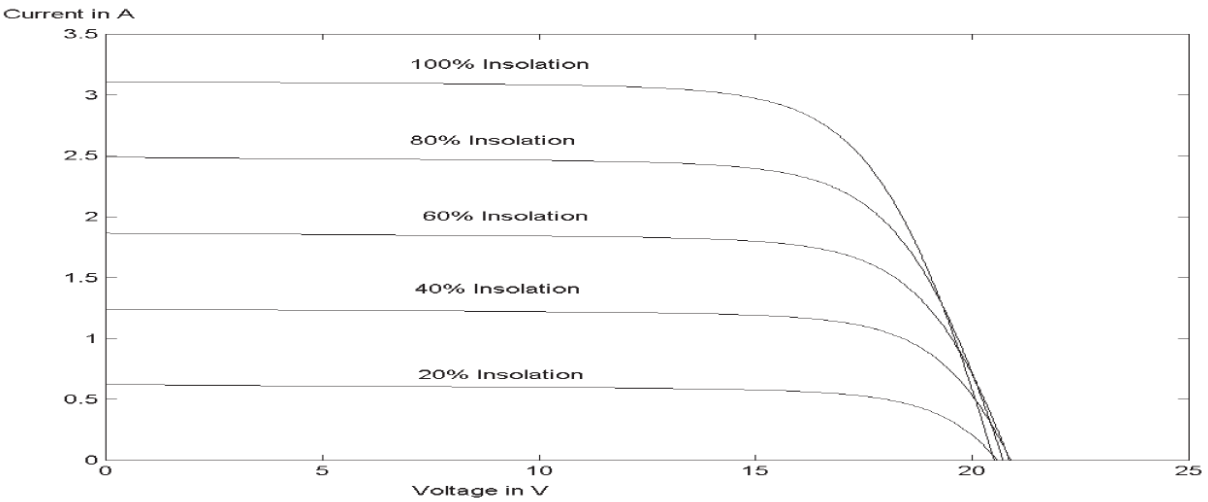

Figure 1.17: Effect of insolation level on V/I characteristic curve of solar panel [37]

Chapter 2

Harmonics in Distribution Network

This chapter presents a comprehensive overview about various voltage source converter topologies, control schemes and their role in harmonic injection. It also discusses the harmonics resonance problem in a distribution feeder which is loaded with dispersed generators. A thorough literature survey on the effects of harmonics on various insulation systems such as machine insulation and cable terminations is also presented. Finally, chapter concludes with the research objectives and the thesis outline.

2.1 Voltage Source Converter (VSC) in Wind and Solar Systems

One of the earlier constraints in the development of solar and wind capacity was the unavailability of high power semiconductor switches. These days high power IGBTs up to a current rating of as high as 3.5 kA and switching frequencies as high as 10 kHz are available. These IGBTs can handle a few MWs of power quite easily. For instance the commercially available converter for wind farms by Siemens under the brand name of DYNAVERT XL can handle up to 8 MW power. Similarly the photovoltaic specific inverter product of Siemens under the brand name of SINVERT is available from 10 kW to MW level.

The prime reason for using converter based interface with the grid is the strict interconnection requirements imposed by the utilities. Almost all the utilities require the wind and solar generator to inject/absorb certain amounts of reactive power. For instance, as per IESO the wind generation facility must be capable of injecting 0.35 per unit of reactive power and absorbing 0.33 per unit of reactive power at the point of common coupling (PCC). The back-to-back inverter configuration allows full control over reactive power. Additionally, if there is a greater requirement of reactive power compensation which varies case by case, utilities suggest installing power electronic based reactive power compensation devices like Static Compensator (STATCOM) and Static Var Compensatior (SVC) which use high switching frequency IGBT switches.

Different semiconductor devices are used depending on the voltage and power level of the inverters. Metal oxide bipolar junction transistors (MOSFET) are preferred for low DC voltages up to 96 V because they have low switching losses at high frequencies and the device voltage drop is only 2 V. However, IGBTs are preferred for high voltage levels [42].

Three types of switching methods viz. square wave, quasi square wave and pulse width modulation (PWM) techniques are used. Usually square wave and quasi square wave switching schemes are used in remote stand alone SPV systems, which are normally used to operate the pumps through an induction machine [43]. The PWM switching scheme has higher switching losses and EMI noise due to high di/dt and dv/dt [44] therefore they require EMI filters which add to the cost of inverters. Such high costs are not justified for remote standalone SPV applications; therefore, square wave or quasi square wave switching schemes are used for such applications.

PWM schemes are the most common ones used in inverters. The output waveform contains variable width pulses generated by the comparison of a modulation and a carrier wave. PWM technique gives full independent control over the amplitude and frequency of the output waveform, and if operated in the under modulation mode, it eliminates the low order harmonics. Moreover, harmonic filters can be easily designed for PWM based inverters because the harmonics generated from a PWM scheme are at well defined frequencies. Fig 2.1 shows typical square and PWM waveforms.

Converter topology is another important design factor. Wind and solar converters use 2-level, 3-level or multi-level converter topologies [45, 46, 47]. A two level VSC consists

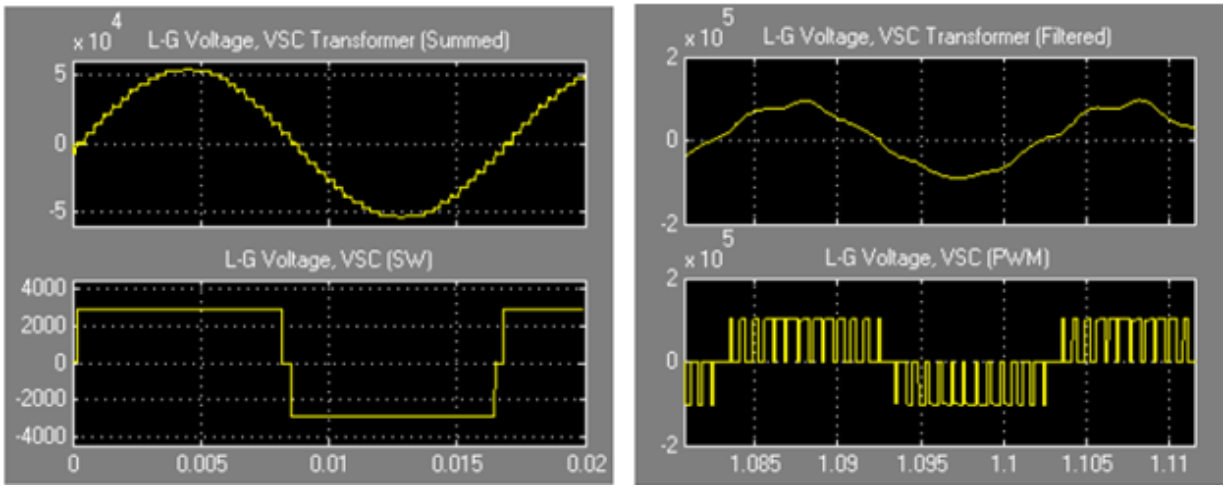

Figure 2.1: A sample square and PWM pulse waveforms

of three identical half bridge inverters as shown in Fig 2.2 [48]. It is called a two level converter because each of the three terminals on the AC side can assume two voltage levels i.e +VDC and -VDC with respect to n point. Power can flow in both directions with this topology. Two level topology is very common in medium and high power applications [49] but the drawback of this topology is that each switch in the converter has to bear full DC voltage in the off state, which requires expensive higher voltage level switches to be used. One way designers handle this problem is to use multiple switches in series. However this approach adds to the complexity of the design. With a multiple switch approach all the switches in one switching cell need to be fired at the same instant, and an additional snubber circuit is also required to divide the voltage equally. At high powers snubber circuits are very lossy which increase the operational cost of the inverter. To overcome such problems, three level or multi-level topologies are used. Although the multi level approach is expensive and complex to implement compared to the two level approach, it gives improved power quality, reduces operational losses due to snubber circuits, and solves the problem of high voltage switches. Fig 2.3 shows a typical multi level inverter output [49]

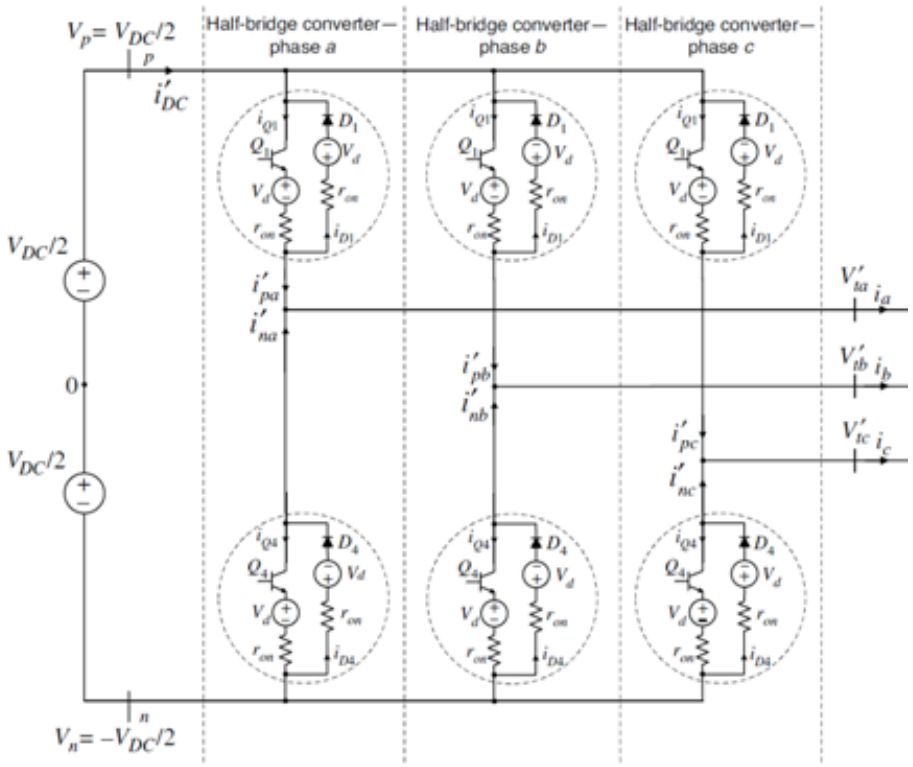

Figure 2.2: Schematic representation of non-ideal 2-level VSC[48]

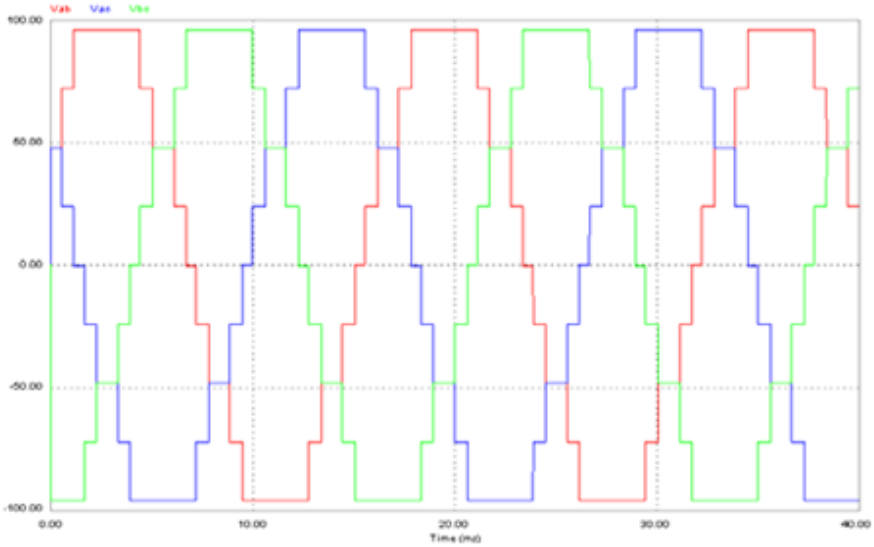

Figure 2.3: Output of a typical multi level inverter[49]

2.2 Harmonic Resonance

Usually utilities put an upper cap on the harmonic injection by interconnecting a renewable generator. North American utilities usually refer to IEEE Standard 519 which allows maximum total harmonic distortion of 5% at any point in time [50]. However this is not always met because the distribution network is now an active system like a transmission network. Distribution feeders have now DGs connected, and it is expected that a single feeder may have multiple DG units, possibly of different types like solar or wind. Earlier, when there were no DGs on the feeder, each feeder had a known group of resonant frequencies for which an appropriate plan could be devised. But this is not true for the feeders with DGs. It is impossible to identify all the resonant points of the feeder because in this case, the system capacitance is dependent on the states of nature, for instance the wind profile in the case of wind farms. So the system resonance is no longer a set of known values. A system can resonate at many frequencies depending on the feeder's operating condition.

Bronzeado, et al. [51] have tried to understand the harmonic emission of a wind farm by measuring the output voltage and current waveforms of the prototype 30kW wind generator, which is connected to a distribution network through a distribution feeder. They have reported a THD of 5-6% in the output current but there was not much effect on the voltage waveform. This was expected because the voltage distortion also depends on the short circuit level of the PCC. If the short circuit level is very high compared to the wind power, then the voltage waveform does not see much distortion. None the less the results in Bronzeado, et al. [51] gives an insight into what would happen to weaker power systems when high power wind parks are connected.

Apart from the amount of distortion, the presence of a wide range of harmonic frequencies increases the probability of resonance in the network. Esposito, et al. [52] have conducted a comprehensive harmonics injection case study on ATP-EMTP commercial software on a 6 kV distribution network to show the presence of wide band of frequencies. A 650 kW power converter based DG connected to a 6 kV bus is simulated in this study. Various harmonic injection schemes are simulated by different switching schemes viz. Sine Pulse Width Modulation (SPWM), Hysteresis Band and Square Wave. The results show that although the THD is within 6.5%, the limit specified by the IEC 61000-3-6 [53], the

individual harmonic limits are violated at the PCC at different frequency levels depending on the switching scheme. For example, for hysteresis commutation the harmonic limits are violated for frequencies between 1 kHz to 2 kHz. Another point of concern is the propagation of harmonics further into the network. In this particular case the harmonics propagated well to a distance up to 4.3 km from the PCC [52].

The harmonic injection may be within the standard limits, but it may become a serious issue if any of the injected frequency resonates with the feeder's resonant frequency. A system can resonate at a certain frequency if at a given location the inductive reactance seen at that point becomes equal to the capacitive reactance. There can be two types of resonance conditions which may happen in a system viz. series and parallel resonance. Parallel resonance shows high impedance to the resonating frequency which results in high voltage distortion at the point of harmonic emission, PCC in the case of wind and solar parks. However series resonance shows low impedance to the resonating frequency which results in high voltage distortion in the whole circuit involved in the series resonance [54].

The resonance may become a serious problem when there are multiple converter based DGs installed on the same feeder. A distribution feeder already has power factor correction capacitors (PFCC) either installed along the feeder or at the substation which itself adds to the resonance of the system. Renewable energy power converter based DGs are connected on the system with a PFCC at their terminals to meet the reactive power requirements laid down by the utilities. Addition of these capacitances not only adds resonance peak at lower frequencies but also shifts the system's original resonant frequency at the capacitor buses as well as at the PCC. The amount of reactive power compensation depends on individual wind generator output. For example, in wind farms spread over a wide area, each wind turbine may not be operating at the same output level as others in the farm. This means that each of them requires a different amount of reactive power compensation to maintain power factor close to unity across their terminals. So there can be many combinations for reactive power compensation depending upon the operating condition of the individual turbine which shifts the feeder's resonance frequencies. In addition to PFCC, the underground cable connection of DGs to PCC is another source of feeder resonance. The cable lengths typically range from two kilometres to twenty kilometres in length [2]. This adds additional capacitive component to the feeder, consequently introducing a resonance peak in the circuit. In summary, a typical overhead feeder which may have single resonance

peak due to PFCCs can have multiple resonance peaks due to the installation of renewable energy generators. These resonance peaks shift depending on the operating condition of the DGs. Because resonant frequencies shift and there is continuous harmonics injection by DGs as discussed earlier, there is high likelihood of system resonance resulting in high voltage distortion.

Varma, et al. [2] carried out a resonance study on a Hydro One feeder with wind turbine generators (WTG) connected to the feeder by overhead lines. It has been shown that at different operating conditions how the resonance peaks shift from one frequency to the other, Fig 2.4 [2], and subsequent harmonics distortions with 1, 2 and 3 wind turbine generators connected to the feeder. The worst case, a THD of 7% in voltage and 40% in

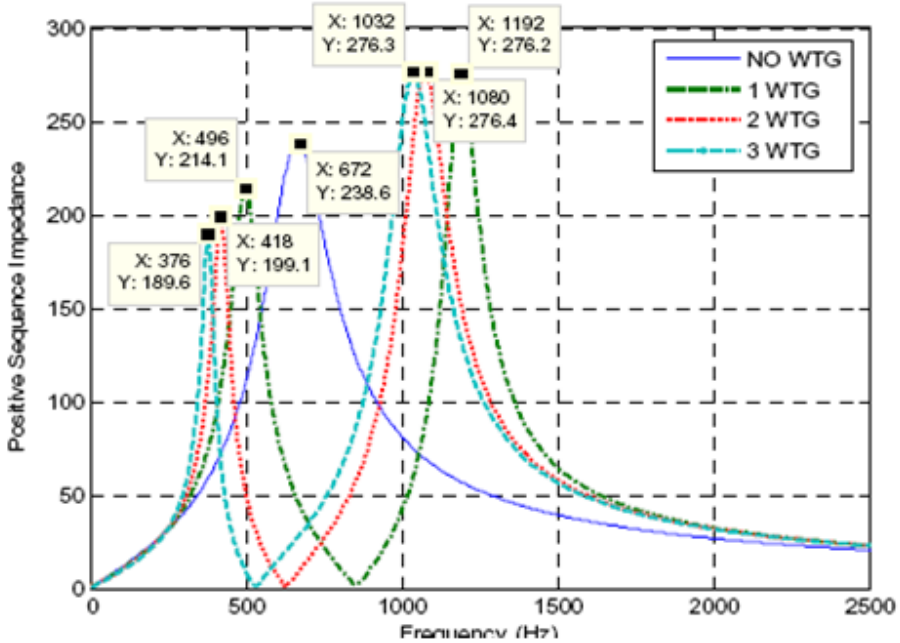

Figure 2.4: Resonance dependence on wind farm operating conditions[2]

current, happens when two wind turbine generators are connected to the system. This is because at that condition the system resonance frequency coincides with one of the injected harmonics by the WTGs.

Many studies have been reported in the literature to show the existence of harmonics resonance conditions occurring due to DGs connected on the feeder [55, 56, 57]. For

instance in [55] the authors have identified a very high harmonics distortion problem due to a series resonance condition appearing close to 11^{th} harmonic on the low voltage side of a 25 MW wind farm. Total harmonic distortion in current reached an alarming high level of up to 38%.

Having identified the harmonic distortion problem in a REDG environment, one may suggest designing a proper filter or appropriate converter switching to mitigate the selective harmonics. However, the continuously changing resonant frequencies of the system make this approach impractical. Standard power system components such s transformers, underground cables, machines etc. are designed to operate under power frequency. Manufacturers provide the estimated life time of these equipments assuming power frequency operation. At this point we are not sure how the insulation system will perform in the high frequency environment. It has now become important to understand the performance of the insulation system under higher frequencies. It will help manufacturers to develop better insulation system designs which can sustain high frequency stresses over the entire duration of equipment's nominal design life. Manufacturers like Allmänna Svenska Elektriska Aktiebolaget, Brown and Boveri (ABB) and General Electric (GE) are already researching into new and improved insulation materials to cope with the high frequency stresses. Also, utilities have changed their approach towards asset management. These days utilities prefer risk based maintenance over the traditional schedule or time based maintenance to reduce the maintenance costs. A better understanding of high frequency stresses will help utility asset managers to assign appropriate risk indices to each equipment which will eventually translate into lower maintenance costs and higher profits to the company.

2.3 Effects of Non-fundamental Frequencies on Insulation Material

The deteriorative effects of high frequencies on insulation degradation have been shown for various power system equipment. However most of the work has been done either on machine insulation [58, 59, 60, 61] or the stress grading of cable terminations [62, 63, 64]. Very little literature is available on the high frequency voltage effect on transformer

insulation.

A recent publication [65] has shown the aging effect of high frequency voltages on the transformer paper insulation. The authors have shown times to breakdown of the impregnated paper insulation under a clean sinusoidal waveform and a 5 kHz 1 kV repetitive impulse superimposed on a 50 Hz sinusoidal waveform. The superimposed waveform is achieved by superimposing independently generated repetitive impulses and clean sinusoid. It has been shown that samples aged under high frequency failed twice as fast as those aged under power frequency.

The distribution level transformers up to 10 MVA have only polyimide coating for turn to turn insulation. The thickness of the coating depends on the voltage level of the transformer, and it is selected based on ANSI/NEMA MW 1000-2003 standard [66]. The literature available on the effect of high frequency repetitive pulses on magnet wire insulation is good representation to show the effects of non-fundamental frequencies on transformer magnet wire insulation. For instance, Grzybowski, et al. [67] have studied the effects of high frequency repetitive pulse aging on three types of magnet wire twisted pair samples. Partial Discharge Inception Voltage (PDIV), partial discharge (PD) level and PD count are used as comparison parameters to see the effects of high frequency repetitive pulse aging. Three magnet wire samples are aged, and each of them was aged for 80 hours at 3200V 40 kHz positive pulse. The results showed a substantial decrease in the PDIV, increase in PD pulse count and PD level after aging.

Sonerud, et al. [68] have associated increased dielectric losses with the distortion level of the voltage waveform. A modified power loss equation is proposed in [68], which also includes the effects of voltage harmonics. This increased dielectric loss also led to the failure of cable termination in Eagle Pass back to back (BtB) installation [69], where one of the injected harmonics got amplified up to 40% of the fundamental voltage leading to the thermal runaway of the cable termination. The study in [68] is distinctive in a way because it has identified that voltage distortion also adds up to the deterioration of the solid dielectric material due increased power losses. This point is missing in most of the literature which studies the effect of harmonics on the transformer insulation [70, 71]. Even the IEEE Standard 519-1992 does not take into account the effect of voltage harmonics on insulation system.

2.4 Research Objectives

The sections above review the harmonics in a DG loaded distribution feeder, their effect on the high voltage insulation system and the test setup used to generate the high frequency superimposed waveforms. It has been found that there is a good understanding of high frequency voltage distortion in HVDC transmission networks. Also, a considerable amount of work has been done to identify the effects of high frequency voltages on various insulation systems such as cable terminations and machine insulation. Despite the rising failure rate of transformers due to high frequency stresses, as reported by CIGRE [72], there is very little work done on transformers regarding high frequency effects. Due to this reason following research objectives are set for this thesis.

- A detailed model of a test distribution feeder is developed on PSCAD/EMTDC^{TM} to understand the resonant frequency shifting phenomenon under variable wind farm operating conditions. This study is performed to prepare a base case for this research
- A partial discharge localization experiment is designed to understand the effects of high frequency on a resin dry type transformer.
- For thorough understanding, a finite element analysis of a high voltage coil is carried out to understand the field distribution under high frequency voltages.
- Finally, an aging experiment is designed to age the impregnanted paper samples of a power transformer under distorted waveforms to understand the impact of high frequency on paper insulation.

2.5 Thesis Outline

The thesis is organized as follows:

- Chapter 1 reviews the concept of distributed generation and some of the common DG technologies i.e. wind and solar generation.

- Chapter 2 discusses various voltage source converter topologies, control schemes and their role in harmonic injection in the distribution feeder. It also presents the harmonic resonance conditions happening due to the variable operating conditions of wind and solar farms and the effects of high frequency on insulation systems such as cable terminations and machine insulation. Chapter 2 concludes with the research objectives defined for this study and the outline of thesis.

- Chapter 3 presents a detailed review on the insulation system of distribution class transformer and provides a comprehensive overview on the harmonic generation test setups.

- Chapter 4 covers the design of IEEE 34 bus distribution feeder on PSCAD/EMTDC^{TM} and simulation methodology and presents the results and discussion on feeder resonance study.

- chapter 5 discusses the design of a partial discharge localization experiment developed to understand the electric field distribution in transformer winding at high frequency. This chapter concludes with the result of PD localization experiment.

- At first, a detailed design of high voltage coil for finite element simulations and its ladder network representation are presented in chapter 6. The ladder network parameter calculation methodology on COMSOL^{TM}, potential distribution calculation on MATLAB^{TM}, electric field computations and its implications are also discussed in this chapter. Finally, the design of experimental setup to study the aging of transformer paper insulation under distorted waveforms is explained and experimental results are presented and discussed in detail.

- Chapter 7 provides the research summary, conclusions and the future work in the area of high frequency effects on transformer insulation.

Chapter 3

Materials and Methods

This chapter presents a detailed description on transformer insulation system. It also discusses various high frequency testing techniques.

3.1 Transformer Insulation System

Modern distribution class transformers are almost always oil filled with paper and press-board insulation between the winding layers. Since it is a multi-dielectric insulation system, one of the design goals of transformer insulation system is to keep the permittivity of the dielectric materials as close to each other as possible. This is because the electrical stress is distributed in inverse proportion to the electrical permittivity. Besides this, the other design objectives are to have as high dielectric strength as practically possible, low loss factor and use of contamination free oil to get the highest possible breakdown strength.

Generally Kraft paper is used as a solid insulation. It is essentially a cellulosic molecule as shown in Fig 3.1, extracted from un-bleached softwood pulp [73]. Softwood generally contains 40-50% of cellulose, the prime component of Kraft paper, which is separated from other components, i.e. 20-30% lignin and 10-20% hemicelluloses and polysaccharides through a sulphate process. In contrast to the sulphite process used for newspaper material, the sulphate process is used because it produces a slightly alkaline residue. Sulphite based processes produce acidic residue which shortens the paper life [74]. The main strength of

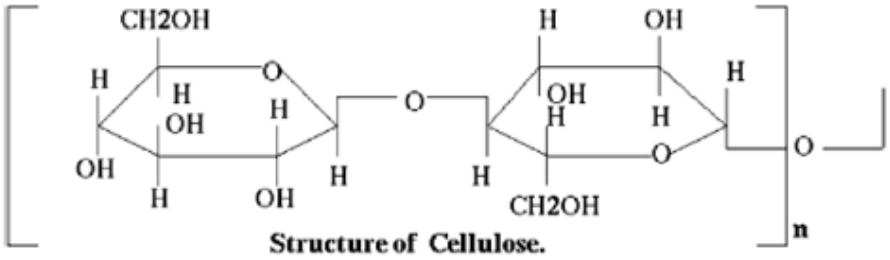

Figure 3.1: Cellulose molecule[73]

the paper comes from the polymeric and fibrous nature of its molecule. For this reason it has now become a well accepted industrial and research practice to find the average number of glucose monomers in cellulose chain by the viscometric degree of polymerization (DP_v) test. For new Kraft paper the DP_v value ranges between 1000-1500 [73]. Over the period due to various aging mechanisms, the average chain length reduces considerably. Literature shows that paper loses much of its mechanical strength at DP_v value of 150 -200 and it is assumed as the end of life of paper insulation [73, 75]. However, there is no mutual consensus over the end of life of criterion. For instance, in [76] Bozzini suggested a DP_v value of 100–150 and Lamp and Carrander [77] suggested a DP_v value of 200 to be the end of life.

Paper degradation is a complex process which mainly happens because of hydrolytic, oxidative and thermal degradation processes. However the effect of each of these degradation processes is the breakage of the glucose chain thus, reducing the mechanical strength. An appreciable amount of work has already been done to identify the paper aging under elevated temperatures [75], and various diagnostic methods have been proposed to identify the condition of paper insulation such as gel permeation chromatography, dissolved gas analysis, degree of polymerization, etc. [73]. However there is very little literature available on electrical aging of paper insulation under non-fundamental frequencies such as in [65].

Besides Kraft paper, cotton is another source of high quality cellulose. Cotton cellulose fibres are larger in length compared to Kraft paper but due to weak intrinsic bond strengths they are not as mechanically tough as Kraft cellulose. Due to the extra absorbing capability of cotton fibres, cotton gives additional electrical strength to the paper insulation. In order

to optimise both mechanical and electrical strength of insulation paper, manufacturers use both Kraft and cotton cellulose. Sometimes other fibres such as manila hemp and jute are used together with cotton and wood fibres to achieve application specific electrical properties such as required for capacitors and cable insulation [74].

Distribution transformer manufacturers also use speciality papers such as crepe paper, thermally upgraded paper and diamond dotted press paper for additional requirements. Crepe papers are crinkled thick paper with a high degree of extensibility. They are particularly suitable to use for hand application of insulation on electrostatic stress control rings, and their high degree of extensibility makes them suitable for uneven surface and bending applications such as joining and forming tapping leads. Thermally upgraded papers are particularly suitable in distribution transformers where the moisture contents and oxygen are relatively high because of a less sophisticated breathing system and lesser maintenance frequency. Moisture and oxygen under operating temperatures increase the insulation aging rate. Thermally upgraded paper does not increase the operational temperature limit of a transformer; however, it significantly reduces the rate of aging due to moisture and oxygen at the operational temperature [75]. Diamond dotted press paper is used in distribution transformers between the winding layers. The resin dots on the Kraft paper give extra mechanical strength to the paper [74].

Paper itself is not a good insulation. It has to be used in combination with oil. The use of oil in transformers is twofold. It increases the dielectric strength of paper insulation and at the same time works as a coolant. The paper insulation is impregnated under special conditions as specified in ASTM D2413-99 (2009) standard. Paper impregnation is a two step process. First the paper is vacuum dried and oil is degassed in a vacuum. Then paper is impregnated with oil in a vacuum to achieve the appropriate impregnation. Transformer temperature rises during normal operation due to iron and copper losses and is limited to 100-110 ^{o}C due to paper insulation. Therefore, it is essential to remove the heat at the same rate as it is generated. The temperature rise determines whether the oil should be naturally circulated or forced through pumps. Usually in distribution class transformers, the oil is circulated naturally.

The distribution class transformers are generally mineral oil filled. Crude petroleum is the only source of mineral oil. Crude petroleum is mainly classified as paraffinic and naphthenic depending on the concentration of paraffin and naphthene hydrocarbons. Paraffinic

hydrocarbons are straight or branched chain hydro carbons as shown in Fig 3.2 [74]. In contrast, naphthenic are cyclic hydrocarbons with single bonds as shown in Fig 3.3 [74]. Naphthenic oils are better in performance than paraffinic oils because they remain in liquid state at temperatures as low as -50 °C and their viscosity changes rapidly with temperature so they can dissipate heat much faster. As identified earlier, oxidation is one of the

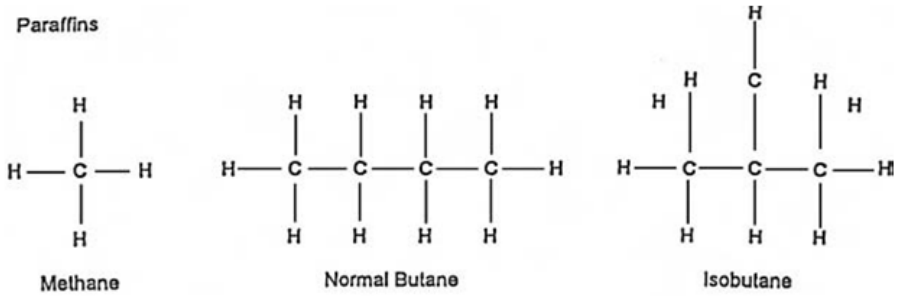

Figure 3.2: Paraffins[74]

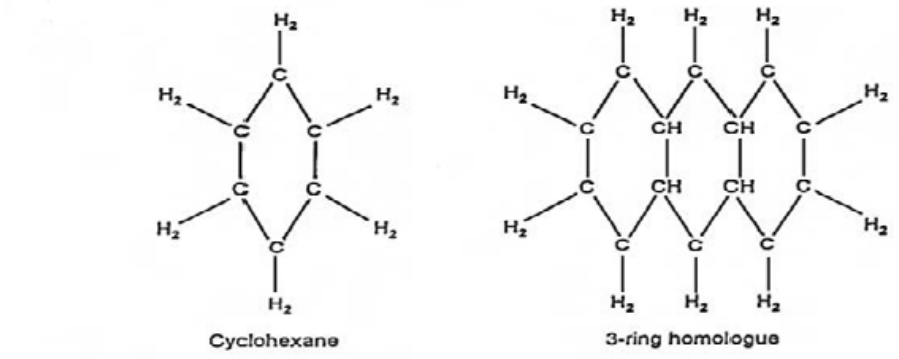

Figure 3.3: Naphthenes[74]

factors of aging of paper insulation. Oxidation mainly forms sludge and increases the oil acidity. Sludge formation hampers the heat dissipation process and results in temperature rise which further increases the rate of oxidation. Increased oil acidity corrodes the metal parts and damages the solid insulation. For this reason oxidation inhibitors are added to reduce the rate of oxidation. Also, pour point depressants are added to paraffinic oils to reduce the pour point of oil so that it remains in liquid state at low temperatures. Paraffinic oils form wax below 0 °C which reduces the heat dissipation ability of the oil.

Due to highly inflammability of mineral oils, they are not preferred in fire hazardous areas. Alternatively, synthetic oils such as esters and silicones are used, which are non-flammable and give equivalent performance compared to mineral oil [74].

3.2 Review of High Frequency Aging Setup

In order to study the behaviour of insulation materials under non-fundamental frequencies, it is essential to design a proper high frequency testing setup. Contrary to typical DC or power frequency, high voltage generation is altogether a different design strategy to produce high voltage-high frequency testing signal. Superposition of non-fundamental frequency on power frequency signal adds another complexity to the design procedure. This section provides an overview of both of these techniques available in the literature.

3.2.1 High Frequency High Voltage Generation

Typically there are three conventional methods available for high frequency generation viz. high frequency transformer method, resonance principle and Tesla transformer method. The easiest and the least complex method is the high frequency transformer method. It is simply the amplification of a low amplitude, high frequency signal to a high amplitude through conventional transformer principle. However, this approach requires special core design with ferrite material. Moreover, such an approach requires impractically high power if samples with capacitances of a few hundred pico farads need to be tested on frequencies of tens of kilohertz [78, 79].

An alternative way is to use the resonance principle in conjunction with a high frequency ferrite core transformer. Usually, the test sample capacitance is a few hundred pico farads which requires an appreciable amount of reactive power from the voltage source. When applying the resonance principle the circuit is tuned to resonate at desired testing frequency using sample capacitance, transformer coil reactance and tuning capacitor or reactor. In this way, the voltage source only need to supply resistive losses of the circuit. This approach significantly reduces the power requirement. The only drawback with this approach is that the stray capacitance of the secondary coil is in the same order of the

sample capacitance. For this reason the transformer itself starts resonating at frequencies around the test frequency which pollutes the test voltage with undesirable harmonics. Therefore this limits the sample size to be tested [79].

Another approach is to use a Tesla transformer double resonant circuit. It has the ability to generate high frequency voltages up to 1MV. The schematic representation of a Tesla doubly tuned circuit is shown in Fig 3.4 [80]. At primary winding a low voltage in the range of ten kilovolts is applied through a capacitance C_1. The spark gap S is triggered at some voltage V_1 which induces self excitation in the secondary coil. Both coils are air core and immersed in oil. It is a very flexible circuit in terms of operational frequency. It can be tuned to operate right from 10 kHz to 100 kHz [80]. However there are disadvantages of this approach as well. The spark gaps have mechanical wear and relatively low switching frequencies compared to semiconductor devices such as MOSFETs. Because the switches do not operate in synchronism with the damped voltage, they result in non-constant amplitude of test voltage. However this problem can be rectified using semiconductor switches by switching synchronously with the test voltage [79].

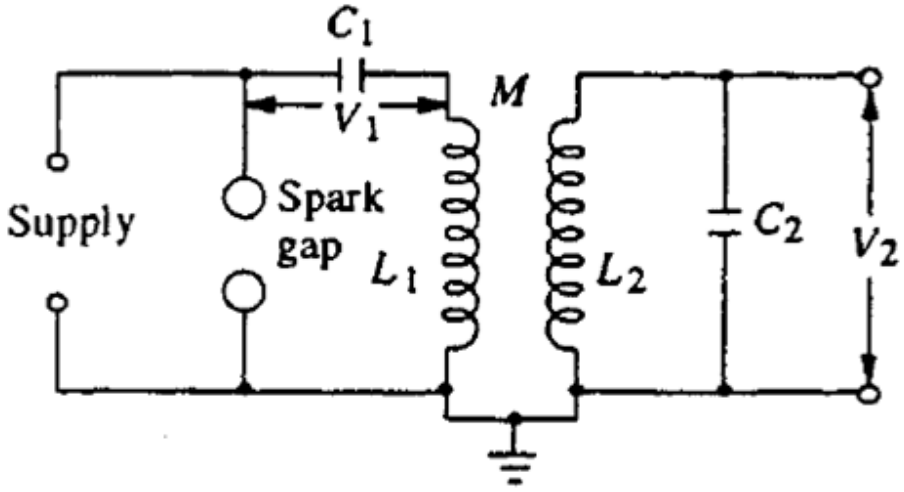

Figure 3.4: Tesla doubly tuned high frequency generator [80]

3.2.2 High Frequency Superimposed on Power Frequency

There are only two ways to generate a distorted high voltage testing voltage. The first approach is to generate the desired distorted waveform at low voltage before feeding it to high voltage transformer. Such an approach has been used by Guastavino, et al. and Montanari and Fabiani [81, 82] to age the XLPE cable insulation samples. This approach is versatile in that there is full control over the distortion level by controlling amplitude, frequency, phase shift and DC offset of each individual harmonic component. This method is used for the experimental work of this thesis. The only drawback of this approach is that it is limited by the transfer function high voltage transformer.

The other approach is to generate and transform the power frequency and high frequency signals separately and then superimpose them at a common node through L and C filter components. Such an approach has been adopted by Paulsson, et al. and Suzuki, et al. [69, 83] to study the aging of cable insulation and terminations. Fig 3.5 shows the schematic representation of such a circuit used by Paulsson, et al. [69] to study the aging of cable terminations. This approach has the advantage that higher order harmonics can

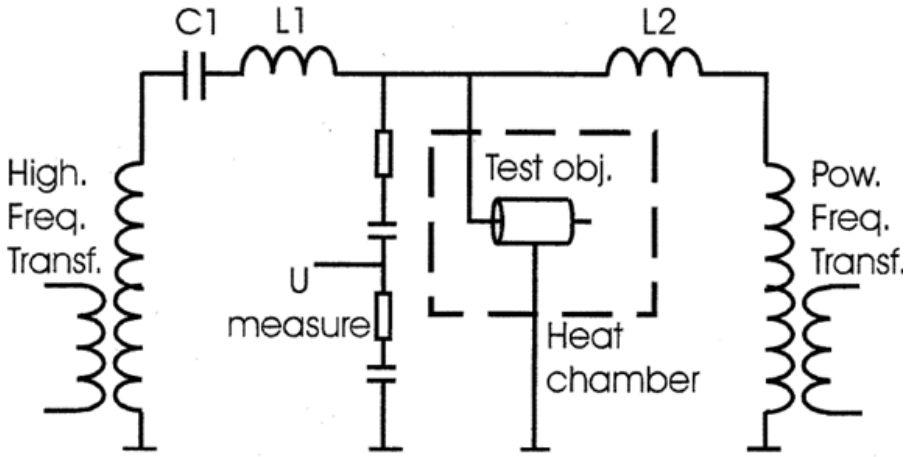

Figure 3.5: PF+HF testing setup[69]

be super imposed on power frequency, which is the limitation of the first method. But this method cannot be used to superimpose low order harmonics (3^{rd}, 5^{th}, 7^{th} etc.) because it is challenging to design a proper filter to protect both transformers from unwanted fre-

quencies. The challenge lies in the closeness of the fundamental frequency and low order harmonics.

Chapter 4

Feeder Resonance Study Simulations

This chapter presents the design procedure of IEEE 34 bus radial distribution feeder [84] developed on PSCAD/EMTDC™ for feeder resonance analysis and the results and discussion on resonance study.

4.1 Problem Formulation

Wind turbine generators affect the feeder resonance points due to power factor correction capacitors and the underground cable capacitances. This may become a potential harmonic distortion problem if there are several types of WTGs connected on the same feeder [2]. As identified earlier, wind and solar farms are themselves not a significant source of harmonic injection [85, 86] but they may become a potential source of harmonic distortion if the feeder resonance coincides with the in-limit harmonic spectrum injected by the connected DGs.

The IEEE Distribution System Subcommittee has proposed a comprehensive 34 bus radial distribution test system comprising all the electrical components representing a real distribution feeder. This system is typically used to perform various power system studies such as load flow analysis, feeder voltage drop calculations under different scenarios, or power quality analysis such as feeder resonance calculations as done in this study etc. In this study, the IEEE-34 bus radial distribution system is modelled in PSCAD/EMTDC™

to study the effect of distributed generators on the feeder resonance under various operational conditions. Each component is modelled with enough detail to get an acceptable level of accuracy [87]. However, some components like regulators and wind turbine models are not included in the study to avoid the complexity to the problem. The bus and line parameters are downloaded from citation [88]. A copy of parameters is provided in Appendix A. The test system is shown in Fig 4.1.

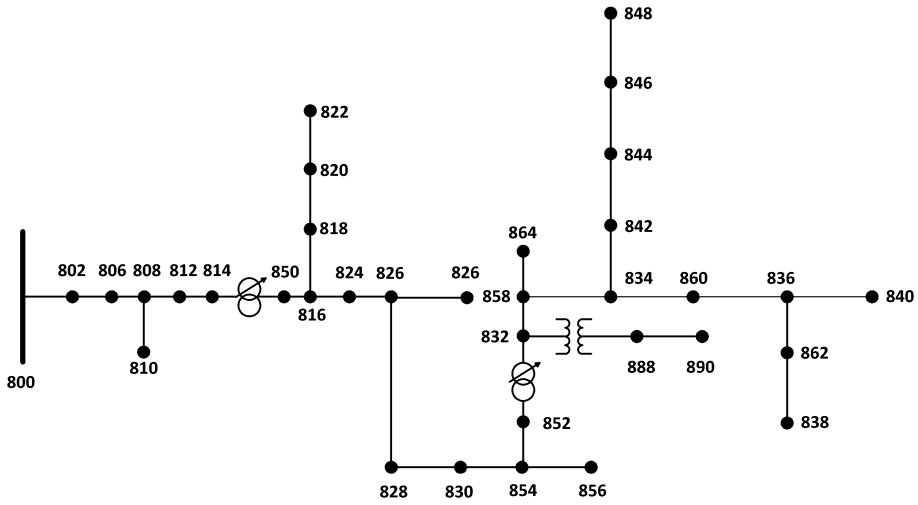

Figure 4.1: IEEE 34 node distribution test feeder[84]

The problem is divided into following:

a. Unbalanced transmission line modeling

b. Distributed load modeling

c. Load modeling (phase and phase to phase load)

d. Wind generator modeling

Two voltage regulators, as shown in Fig. 4.1, between nodes 814 and 850 and 852 and 832 are not included in the model because it only adds to the complexity of the system without adding any value to the study itself.

A new block was developed to model unbalanced transmission lines using mutually coupled wires because there are no pre-built models of unbalanced transmission lines in the PSCAD/EMTDC^{TM} master library. PSCAD/EMTDC^{TM} gives full liberty to individually define the mutual coupling among the lines. The Z and B coupling matrices, shown in Appendix A, for each configuration from 300 to 305 are used to define the coupling among the phases.

The spot and distributed loads are modelled in a different manner. Distributed loads are modelled using the exact lumped load model discussed in Santoso and Zhou [89]. One third of the load is connected at the end of the line and the other two thirds are connected at one fourth the distance from the source. On the other hand, the spot loads are modelled by the built in load model in the master library.

For each distributed and spot load there are three kinds of loads to be modelled viz. constant power, constant current and constant impedance. All of the three types are modeled by the fixed load model from PSCAD/EMTDC^{TM} master library. PSCAD/EMTDC^{TM} models this block by widely accepted load model equations (4.1) and (4.2) which are functions of voltage and frequency,

$$P = P_0 \cdot \left(\frac{V}{V_0}\right)^{NP} \cdot (1 + K_{PF} + dF) \tag{4.1}$$

$$Q = Q_0 \cdot \left(\frac{V}{V_0}\right)^{NQ} \cdot (1 + K_{QF} + dF) \tag{4.2}$$

where,

P=Equivalent load real power per phase
P_0=Rated real power per phase
V=Load Voltage (RMS, L-G)
V_0= Rated load voltage (RMS, L-G)
NP = $\frac{dP}{dV}$=Voltage index for real power
K_{PF}=$\frac{dP}{dF}$= Frequency index for real power
Q=Equivalent load reactive power per phase

Q_0=Rated reactive power (+inductive) per phase
NQ = $\frac{dQ}{dV}$= Voltage index for reactive power
K_{QF}= $\frac{dQ}{dF}$= Frequency index for reactive power

Appropriate values for NP, NQ, K_{PF} and K_{QF} as shown in Table 4.1, are selected from Kundur [90] to model the constant PQ, constant Z and constant I loads. In PSCAD/EMTDC™ by default the load stays in constant impedance form until 10 cycles are passed. Factor dF is programmed to be the minimum of 10, $90/K_{PF}$ and $90/K_{QF}$. If dF is outside this range then load automatically reverts back to constant impedance form. Phase to phase loads are modelled by variable resistors and inductors in parallel. Their value is updated at each time step.

Table 4.1: Load Parameters [90]

Load Type	NP	NQ	K_{PF}	K_{QF}
Constant PQ	0	0	0	0
Constant Z	2	2	0	0
Constant I	1	1	0	0

Wind generators are modelled by the wound rotor induction machine model available in the master library of PSCAD/EMTDC™. The objective of this study is to show the feeder resonance shifting at various wind generators' operating conditions; therefore, no effort was made to make a detailed wind turbine model which is required when fault ride through studies are required. Instead the input torque was set to a constant value of -1 p.u. which is a fairly good assumption for this study. Additionally, the machine is started in speed control mode and then after 0.1 seconds when machine transients are damped, it is switched into torque control mode.

4.2 Simulation Procedure

System frequency scan is carried out at bus 840 with and without wind generator to identify the shift in feeder resonance points at bus 840. Two simplified wind generator models

Table 4.2: Simulation Test Cases

Simulation Case	WTG 1 - % output	WTG 2 - % output
A	0	0
B	100	0
C	50	0
D	50	100

as discussed in Section 4.1 are connected at bus 840 one by one in different combinations. Table 4.2 shows various wind turbine generator (WTG) loading conditions assumed in this study. The maximum power level of each wind generator was chosen to be 660 kVA. The reactive power consumption of the wind generator depends on the output level of the generator. Therefore, the amount of reactive power compensation would vary accordingly. Hence in this study different loading combinations of two WTGs are simulated and accordingly the reactive power is supplied to keep the power factor at unity. Under each simulated condition, frequency scan is carried out at bus 840.

4.3 PSCAD/EMTDC^{TM} Simulation Results and Discussion

Figure 4.2 presents the results of frequency scan carried out on the distribution feeder with a different number of wind turbines operating at variable loading conditions. The frequency scan results in Fig 4.2 shows that feeder resonant points are affected by wind turbine generators having power factor correction capacitors (PFCC) across their terminals. It is observed in Fig 4.2 that the first resonance peak of the feeder is reduced as the number of wind turbines are increased on the feeder. Also, the second resonant peak tends to move towards higher frequencies with the increase of wind turbine generators (WTG).

Wind farms spread over a wide area and wind profile is not constant over the entire farm; therefore, each wind generator operates at a different power output. This condition is simulated by operating wind generators at different power outputs such as 100%, 50% or a combination of 100% and 50%. The reactive power requirements of each generator depend

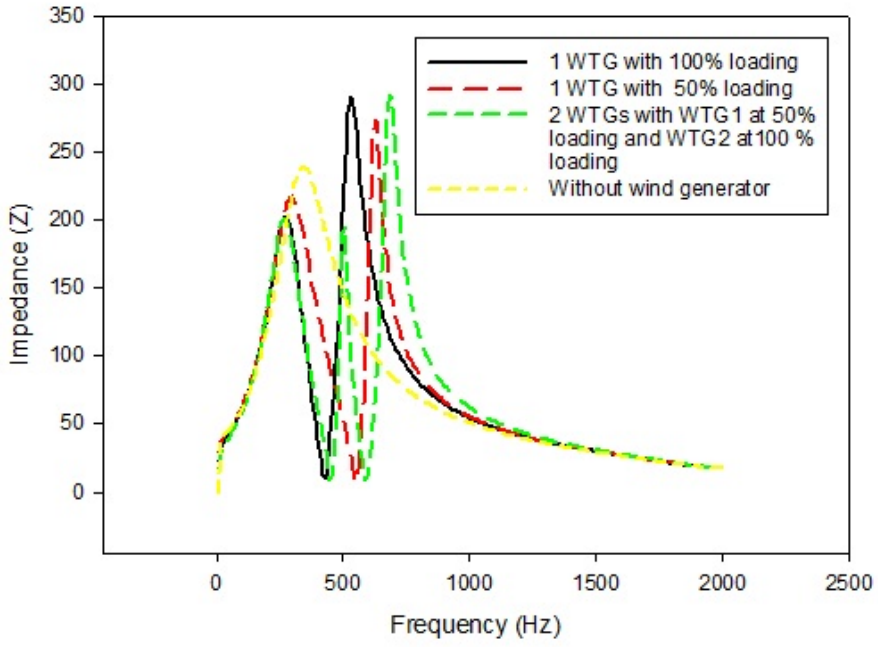

Figure 4.2: Frequency scan plots at bus 848

on the power output of the generator. It implies that a different amount of capacitance is required for each generator for maintaining the power factor close to unity across its terminal.

It is interesting to note from Fig 4.2 that when wind generators operate at different power output levels a third resonance peak is introduced in the middle of first and second resonance peaks. In this study there is one middle peak only because there are only two WTGs considered in this study. The first peak corresponds to the feeder's original resonance. The other two peaks correspond to each WTG. Multiple peaks show up when each wind generator is operating at a different power level which is true for a real wind farm. As shown in this study, because of the resonance shifting, the feeder resonance becomes stochastic; therefore, it is expected that such operating conditions show a potential harmonics distortion problem in the feeder. Also, due to the stochastic nature of the resonance it is very difficult to design an appropriate filter to eliminate harmonics.

The feeder resonance simulation results provide an impetus to investigate the effects

of high frequency on transformer insulation. In this regard several experiments and simulations are carried out in this thesis. As we know that electric field distribution in the transformer winding is hyperbolic under standard 1.2/50 μs transient impulse, so it was expected that electric field distribution in the winding would be different at higher frequency compared to power frequency. To start with this assumption a partial discharge localization experiment was designed whose details are presented in the next chapter. The objective of this experiment was to find out the re-distribution of electric field by identifying the change of partial discharge location using acoustic emission technique.

Chapter 5

Partial Discharge Localization by Acoustic Emission Technique

This chapter presents the details of acoustic emission technique developed to understand the distribution of electric field at high frequency in a transformer winding. This method utilizes partial discharge localization at high frequency to identify the electric field concentration spots in the winding.

5.1 Experimental Procedure and Setup

A test setup is designed to study the effects of high frequency distortion in voltage waveform due to feeder resonance as discussed in earlier sections. A resin dry type transformer, shown in Fig 5.1, is tested under no load condition. The transformer is stressed with 60 Hz and 1kHz voltage waveforms. Under each test condition the partial discharge location is approximated by the acoustic emission (AE) method. A change in partial discharge location would indicate field redistribution at higher frequencies. High voltage winding is stressed according to the IEC 60726 standard for partial discharge measurement. According to the standard, voltage should be applied on the low voltage winding of the transformer, and partial discharge measurements should be performed at high voltage winding [91]. Fig 5.2 shows the test circuit proposed by the standard. As shown in Fig 5.2 the high voltage

Figure 5.1: 100/10,000 V, 10 kVA resin dry-type transformer

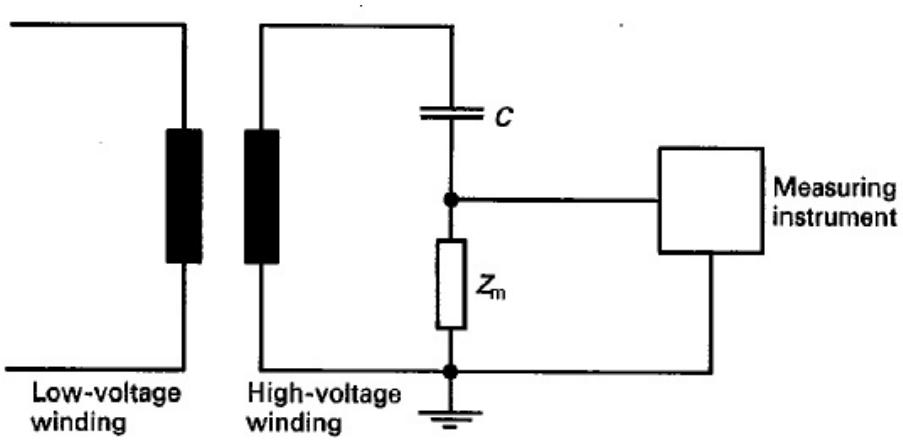

Figure 5.2: Partial discharge measurement test circuit proposed in IEC 60726 [91]

winding, which is a test sample in our study, is connected through a coupling capacitor to a measuring impedance Z_m. Coupling capacitor and measuring impedance are used if one wants to quantify the partial discharge but it was not the objective of this study. Instead, the intent is partial discharge localization which can be done by AE technique. For PD localization High voltage winding is stressed according to IEC 60726.

It is not easy to sense the partial discharge acoustic signal in a resin dry type trans-

former, specifically if it is happening in the inner layers of high voltage winding. The acoustic impedance of materials determines the transmission of signal from one medium to another. For example, for the sake of explanation consider Fig 5.3. An acrylic resin layer is sandwiched between copper blocks representing the high voltage winding. The acoustic impedance, Z = ρV, of copper is 41.66×10^6 kg/m^2·s and of resin is 3.2×10^6 kg/m^2·s. Such a large difference in acoustic impedances means a very high reflection coefficient which can be determined by (5.1). For this example, it is approximately 73.5%. It means that when the acoustic signal transmits from one medium to another, then approximately 73.5% of the signal is reflected back. This concept is explained in Fig 5.3 when an acoustic signal initiating from copper with a signal strength of 100% propagates into resin, 73.5% of it is reflected back and only 26.5% is transmitted to resin. Again, when 26.5% of the original acoustic signal received at resin tries to propagate into copper, 73.5% of it i.e. 19.4% is reflected back and only 7.1% propagates into copper.

Figure 5.3: Acoustic signal trasnmission in copper-resin system

$$R = \left(\frac{Z_1 - Z_2}{Z_1 + Z_2}\right)^2 \tag{5.1}$$

Z_1 and Z_2 are acoustic impedances of the respective materials.

A Plexiglas rod waveguide is used to solve the signal attenuation problem. The selection of waveguide material is done based on the research of Harold [92]. According to Harold [92], Pyrex glass rods and epoxy-fibre glass rods have the minimum acoustic attenuation. The author correlated the transmission coefficient with Poisson's ratio of the material and

found that best performance i.e. attenuation of less than 3dB/m, can be achieved if the Poisson's ratio of the material is less than 0.26. The Poisson's ratio of Plexiglas is 0.4, therefore, the waveguide performance is not as good as Pyrex glass rod whose Poisson's ratio is 0.24. Although, the Plexiglas gain is half compared to the Pyrex rod, the difference does not measurably affect this study; hence, Plexiglas was used.

The working principle of the partial discharge localization is very simple. A Plexiglas waveguide with an acoustic sensor at each terminal is attached on the surface of high voltage winding as shown in Fig 5.1. The sensor signal is fed to a 46dB pre-amplifier before connecting it to the oscilloscope. The sensor has a flat frequency response in the range of 23-80 kHz. The reproducibility of acoustic coupling of the sensor is verified according to the ASTM E976-00, 2000 standard. The standard requires simulating the ultrasonic signal to test the sensitivity of the sensors. Ultrasonic signal is simulated by Hsu-Nielsen source which is a 0.3 mm 2H pencil lead. The pencil lead is broken on the surface of the HV winding. It will generate an ultrasonic signal which should be detected at the acoustic sensors. A 100 mV acoustic signal is detected on the oscilloscope which shows a good acoustic coupling.

The partial discharge localization principle is simple. Let's suppose a partial discharge source is x meters away from the center of the waveguide and the total length of the waveguide is L meters as shown in Fig 5.4. The partial discharge location can be approximated from the equation stated in (5.2).

$$x = V_{Plexiglas}\frac{\Delta t}{2} = 1552\frac{\Delta t}{2} \tag{5.2}$$

Equation (5.2) can also be used to calculate the speed of ultrasound in Plexiglas. An ultrasonic source is placed close to one of the acoustic sensors and Δt is noted on oscilloscope. Δt will be equal to the travelling time of ultrasound from one sensor to another because the ultrasound source is placed beside one of the sensors. x will be equal to half of the distance between two sensors. By inserting these two values in the equation above (5.2), $V_{Plexiglas}$ is found to be 1552 m/s.

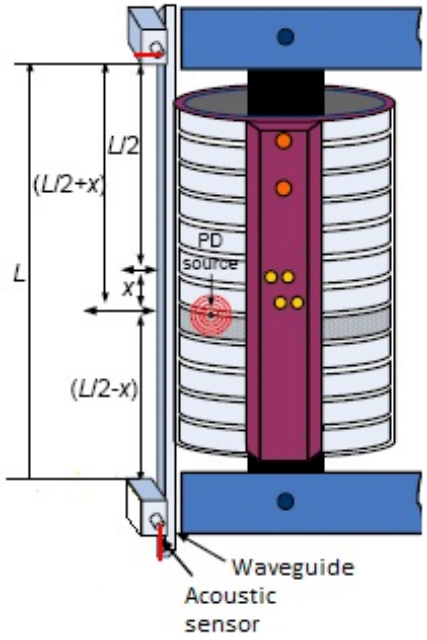

Figure 5.4: Schematic representation of HV winding for PD location measurements [93]

5.2 Partial Discharge Localization Results

This section presents the results of the partial discharge localisation experiment, performed on a resin dry type transformer. The transformer was energized under power frequency, i.e. 60 Hz and 1 kHz high voltage waveforms. 100 V was applied at the low voltage winding of transformer which induces 10kV on the high voltage winding. Under each test condition partial discharge location was identified using acoustic sensors. A Plexiglass acoustic waveguide was attached on the high voltage winding of the transformer. Acoustic sensor attached at the terminals of the waveguide sense the ultrasonic acoustic wave generated by the partial discharge under each test condition, Fig 5.5 and Fig 5.6. The difference in arrival time, Δt, was noted on the oscilloscope to calculate the partial discharge location in the winding using equation (2.4). Δt for 60 Hz waveform was found to be 68 μs, Fig 5.5, which corresponds to a PD location 5.2 cm away from the center of the waveguide. However, when energised by 1 kHz waveform, Δt was found to be 31 μs, Fig 5.6, which corresponds to a PD location of 2.4 cm away from the center of waveguide. The results show a shift in the position of partial discharge at higher frequency which indicates that electric

field inside the transformer redistributes at higher frequency; consequently, localized field enhancement takes place at some other location.

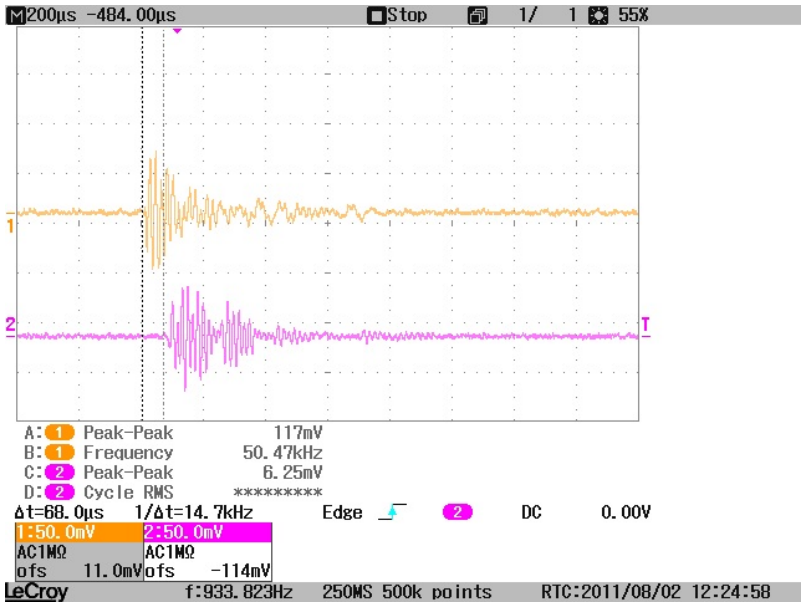

Figure 5.5: Acoustic partial discharge signals received at 60 Hz

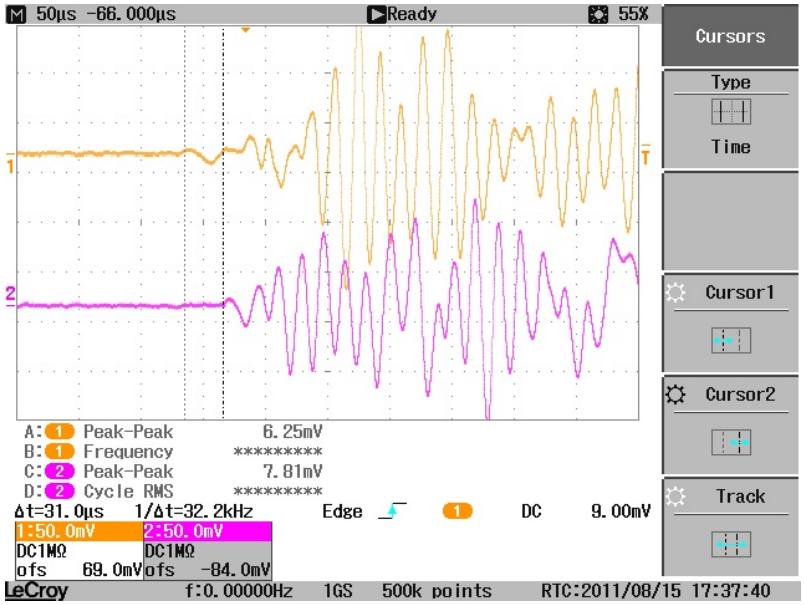

Figure 5.6: Acoustic partial discharge signals received at 1kHz

Chapter 6

Electric Field Analysis and High Frequency Aging

This chapter presents the details of high voltage coil geometry designed to further study the high frequency effect, ladder network representation of coil, and the methodology of finite element model development of the high voltage coil. Lastly, a high frequency aging experiment is discussed, which is designed to study the effects of high frequency distortion on transformer insulation. Results and discussion on each study type are also presented.

6.1 High Voltage Coil Simulations

It has been found in lab experiments that partial discharge location changes at higher frequency. This means that at higher frequencies the field inside the transformer redistributes itself and the localized field enhancement takes place at some other location; hence partial discharges appear at such location. In order to verify this phenomenon, electric field simulations are carried out in COMSOL^{TM} on a small scale high voltage air core coil model. The coil is representative of a typical 45 kV distribution class transformer designed by a local transformer manufacturer.

In this study the high voltage air core coil is defined by an R, L and C lumped parameter network, consequently, coil is completely defined by a set of first order linear ordinary

differential equations (ODE). The R, L and C parameters are calculated by COMSOL^{TM}, finite element software. Once these parameters are calculated, they are used to solve for the circuit node potentials by numerically solving the set of ODEs. From the knowledge of node voltages, electric field calculations are carried out in COMSOL^{TM}.

6.1.1 Coil geometry

Fig 6.1 shows the COMSOL^{TM} model of air core test coil designed for the field distribution study. Coil geometry is drawn in 2D axis symmetric cylindrical co-ordinates, where **z** is axis of symmetry. A prototype 5kV high voltage (HV) coil was designed by a transformer manufacturer considering the actual electrical stresses present in a distribution class transformer. The coil consists of five layers of 30# AWG copper winding, starting from ground potential at the bottom of the innermost layer and terminating at high potential at the top of outermost layer. Each inner layer consists of 371 turns while the outer layer consists of 183 turns. Three layers of PUCARO insulation paper are provided between adjacent coil layers except between layers 4 and 5. Two extra layers of 4 mil insulation paper are

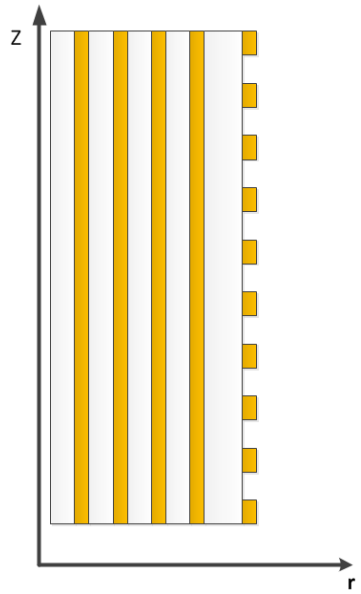

Figure 6.1: Coil geometry - figure not drawn to scale. All golden strips represent coil domains and white strips in between are the insulation layers.

provided between the 4^{th} and 5^{th} winding layer to accommodate the higher stresses during fast impulses. Design details are attached in Appendix B.

6.1.2 Detailed Equivalent Circuit

The coil geometry discussed in the previous section is represented by a lumped parameter R,L and C ladder network shown in Fig 6.2. The ladder network can be completely defined by a set of linear first order ODEs as shown in (6.1) and (6.2). The R, L and C parameters are calculated by the finite element method (FEM) discussed in subsequent sections. The coil is divided into 14 multi-turn coil domains and each domain is assumed as an equipotential surface. Each node in the equivalent circuit represents the equipotential surface. The capacitances connected between each pair of nodes represent the mutual capacitance between adjacent coil domains. The self inductances are in series with the winding resistances representing the winding loss. Mutual inductances are shown by the dotted double arrow which shows the inductive coupling among the coil domains. All mutual inductances are not shown for the sake of clarity.

$$[v_i - v_j] = [R_{ii}]\, i_i + [L_{ij}]\, \frac{di_i}{dt} \quad \forall \quad i, j = 1 \cdots 14 \tag{6.1}$$

$$[i_i - i_j] = [C_{ij}]\, \frac{d(v_i - v_j)}{dt} \quad \forall \quad i, j = 1 \cdots 14 \tag{6.2}$$

6.1.3 High Voltage Coil Finite Element Model

The modelled coil consists of 1667 turns; therefore, it is impractical to model all the turns. If all 1667 turns are modelled, the simulation becomes heavy in terms of memory usage, and the solution time increases by many folds. Even 4GB of memory cannot handle this much detailed model. Therefore, the entire coil is divided into fourteen sections as shown in Fig 6.1. The yellow sections represent the coil domains. Each section represents a group of turns. More detailed modelling is done on the outermost layer of the winding since more stress is expected at the outer most layer. The fifth layer is divided into ten sections, each representing 18.3 turns. For inner layers each layer was modelled by single domain representing 371 turns.

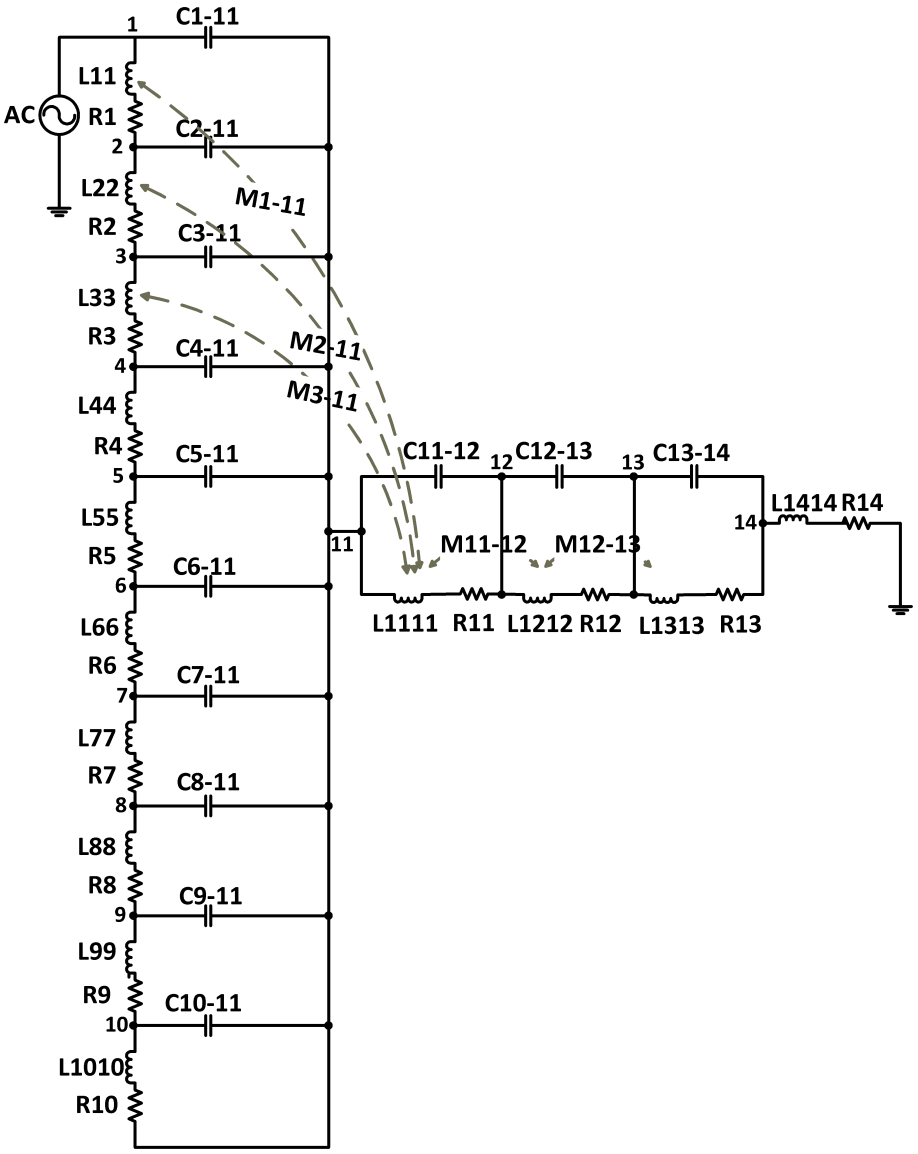

Figure 6.2: RLC lumped parameter model

6.1.3.1 Inductance Calculations

Magnetic fields (mf) physics is chosen to calculate the inductance matrix because it is purely a magnetic phenomenon. Since each domain is representing a multi-turn coil, care was taken to correctly model the multi-turn coil domain. This objective was achieved by assigning external current density to the right hand side of the equation in (6.3), $\sigma=$

Electrical conductivity, ε_0= *permittivity of free space*, μ_0= *permeability of free space*, $\mathbf{A}$= *Magnetic vector potential*, $\mathbf{M}$= *Magnetization field*, $\mathbf{J}^{\mathrm{e}}$= *External current density.* The total current in the coil is proportional to the number of turns in the coil. For example, if each turn is carrying 1 A then a coil domain containing 18.3 turns would carry a total current of 18.3 A. The current density is calculated accordingly. Also, conductivity of the multi-turn coil domain is set to zero in **r** and **z** direction to simulate the inter-turn insulation [94]. The turn cross-section is very small compared to the cross-section of the coil domain; therefore, skin and proximity effect will not show up at frequencies of interest. External density is calculated by the equation in (6.4). In this equation N= *Number of turns*, $\mathrm{I_{COIL}}$= *Current per turn*, A= *Conductor's cross-sectional area.*

$$\left(j\omega\sigma - \omega^2\varepsilon_0\right)\mathbf{A} + \nabla \times (\mu_0 \nabla \times \mathbf{A} - \mathbf{M}) - \sigma \mathbf{v} \times (\nabla \times \mathbf{A}) = \mathbf{J}^e \tag{6.3}$$

$$\mathbf{J}_e = \frac{N I_{COIL}}{A} \tag{6.4}$$

Permeability of other domains i.e. transformer oil and paper insulation is set to permeability of free space because they are not ferro-magnetic materials. The inductance matrix can be calculated in numerous ways. One of the ways is to use the basic definition of inductance as defined in (6.5)

$$L_{ij} = \frac{\phi}{I_i} = \frac{\int\int_{s_j} \mathbf{B} \cdot \mathbf{n} dS}{I_i} \tag{6.5}$$

ϕ is the total flux intercepted by the coil. It is defined as the surface integral of the flux density normal to the area enclosed by the coil as shown in (6.5), and $\mathrm{I_j}$ is the total current in the $\mathrm{j^{th}}$ coil.

This approach is discarded because the flux calculations require definition of the flux intercepting surface. Such a surface definition is difficult to achieve with the coil geometry shown in Fig 6.1. This difficulty can be avoided by a little manipulation of equation (6.5). Surface integral is transformed into line integral by using magnetic vector potential. Magnetic flux density, B in (6.5) can be replaced by (6.6)

$$\mathbf{B} = \nabla \times \mathbf{A} \tag{6.6}$$

Therefore (6.5) can be written as (6.7)

$$L_{ij} = \frac{\int\int_{S_j} (\nabla \times \mathbf{A}) \cdot \mathbf{n} dS}{I_i} \tag{6.7}$$

Applying Stoke's theorem on (6.7) which states that a surface integral of the curl of a field equals the closed line integral over the rim of the surface, equation (6.7) can be transformed into line integral form as shown in (6.8), which is fairly easy and fast to calculate in any finite element software. But this approach is also discarded as it is not accurate enough because the magnetic vector potential is not uniform along the periphery of the turn cross-section and one has to average the magnetic vector potential along the outside edge which induces inaccuracy in the results.

$$L_{ij} = \frac{\oint_{\Gamma_s} \mathbf{A} \cdot \mathbf{t} dl}{I_i} \tag{6.8}$$

In equation (6.8), $\mathbf{t}$=(t_x,t_y,t_z) is the unit tangent vector of the curve Γ_s and dl is an infinitesimal line element.

Another method is the induced potential technique which is similar to magnetic vector approach. This method requires the calculation of induced potential in a coil by taking line integral of the electric field along the coil perimeter. Once induced voltage is calculated, equation (6.9) can be used for inductance matrix computation. V_{ind} is calculated by taking line integral of electric field along the rim of the coil.

$$L_{ij} = j\frac{V_{ind}}{\omega I_j} \tag{6.9}$$

This method is also faster and easy to apply but lacks accuracy much like the magnetic vector potential method discussed earlier.

The most accurate and reasonably faster method is the magnetic energy method. This method utilises magnetic energy computation over the entire geometry. At a time either

single coil or two coils are excited depending upon the type of inductance being calculated, i.e. self or mutual inductance. But mutual inductance calculations require self inductances of the coils in calculation; therefore, all self inductances are computed before any mutual inductance is calculated. Equations (6.10) and (6.11) are used for self and mutual inductance calculations [94].

$$L_{ii} = \frac{2}{I_i^2} \int_{\Omega} W_m d\Omega \quad I_j = \begin{cases} 0 & j \neq i \\ I_i & j = i \end{cases} \tag{6.10}$$

$$L_{ij} = \frac{1}{I_i I_j} \int_{\Omega} W_m d\Omega - \frac{1}{2} \left(\frac{I_i}{I_j} L_{ii} + \frac{I_j}{I_i} L_{jj} \right) \quad I_k = \begin{cases} 0 & k \neq i, j \\ I_i & k = i \\ I_j & k = j \end{cases} \tag{6.11}$$

6.1.3.2 Capacitance and Resistance Calculations

Like inductance calculations, capacitance can also be determined by several methods. It is very easy to calculate the capacitances of simple geometries by analytical formulas. But for complex geometries like a multi-conductor system in this study, it is almost impossible to calculate the mutual capacitances by analytical formulas. For such systems the finite element method (FEM) is quite suitable. FEM is convenient because it can compute the total electrical energy present in the electric field; consequently, capacitances are easily calculated with a high degree of accuracy. The electrical energy method is similar to the magnetic energy method for inductance computations, discussed in Section 6.1.3.1. Capacitances are computed by the equations in (6.12) and (6.13). Appropriate material permittivities are selected from M.J Heathcote [74], 2.2 for transformer oil and 4.4 for paper insulation. Mutual capacitances between the adjacent coil domains are computed for this study because the mutual capacitances between the non-adjacent coil domains are approximately ten times smaller than adjacent ones [95].

$$C_{ii} = \frac{2}{V_i^2} \int_{\Omega} W_e d\Omega \quad V_j = \begin{cases} 0 & j \neq i \\ V_i & j = i \end{cases} \tag{6.12}$$

$$C_{ij} = \frac{1}{V_i V_j} \int_{\Omega} W_e d\Omega - \frac{1}{2}\left(\frac{V_i}{V_j} C_{ii} + \frac{V_j}{V_i} C_{jj}\right) \quad V_k = \begin{cases} 0 & k \neq i, j \\ V_i & k = i \\ V_j & k = j \end{cases} \tag{6.13}$$

Resistance of each coil is calculated one by one with only one coil energised at a time. Equation (6.14) is used to calculate the coil resistances.

$$R_{coil} = \frac{N L \rho_{coil}}{a_{coil}} \tag{6.14}$$

6.2 Electric Field Calculations

The first order ODEs, described in Section 6.1.2 are solved for node potentials in MATLAB™ using the Runga Kutta numerical algorithm. Once all the node voltages are calculated then electric field calculations are done in electric currents physics interface in COMSOL™ under frequency and time dependent study types. Frequency and time dependent study types account for both conduction and displacement currents. Electric currents physics combine the time harmonic equation of continuity in (6.15) with the equation in (6.16) to calculate the electric potential using the equation in (6.17). For time dependent study the same equations are used with all $j\omega$s replaced by time derivatives.

$$\nabla \mathbf{J} = \nabla \cdot (\sigma \mathbf{E} + \mathbf{J}^e) = -j\omega\rho \tag{6.15}$$

$$\nabla \cdot \mathbf{D} = \rho \tag{6.16}$$

$$-\nabla \cdot ((\sigma + j\omega\varepsilon_0)\nabla V - (\mathbf{J}^e + j\omega\mathbf{P})) = Q_j \tag{6.17}$$

6.3 Finite Element Electric Field Simulation Results and Discussion

The results shown in Section 5.2 indicate that there is an electric field redistribution at higher frequencies which causes the localized field enhancement at another place in the winding, causing partial discharge to appear at a different location. In order to further understand the electric field distribution in a transformer, a high voltage air coil was simulated in COMSOL^{TM} for electric field calculations. This section presents the results of all the intermediate steps required for electric field calculations i.e. R, L and C parameters. It also presents and discusses the node potential and electric field results.

6.3.1 R, L and C Parameters

Tables 6.1, 6.2 and 6.3 show the calculated R, L and C parameters. The capacitance table only shows the mutual capacitances between the adjacent coil domains. Since there is no grounded core and tank wall in this coil system, self capacitances are also negligible, hence ignored. Capacitances are evaluated by calculating the stored energy in the electric field between the adjacent coil domains.

All mutual and self inductances are significant; therefore, accurate calculations are necessary for the coil model. For this reason the entire inductance matrix is calculated. Resistances representing the winding losses are frequency dependent but in this particular study they are assumed constant due to thin cross-section of the conductor. Core losses are also ignored in the model because it is an air core coil. Eddy current losses are estimated by Ye Liu [95] (6.18). In equation (6.18), f= frequency, B_m= peak flux density, t= lamination thickness, ρ= resistivity of the core, d= density in kg/m^3.

$$P_e = \frac{1.6 f^2 B_m^2 t^2}{\rho d} \tag{6.18}$$

For air core coils, ρ is very high compared to iron core; therefore, eddy current losses are very small in air core coils. Furthermore, as rule of thumb hysterisis losses are three times smaller than eddy current eddy current losses, hence, very small if the eddy current

losses themselves are very small. Therefore, both of these core losses are not included in this study.

Table 6.1: Resistance of coil domains of high voltage air core coil mode. All resistances are in ohms

R_1	R_2	R_3	R_4	R_5	R_6	R_7
0.5664	0.5664	0.5664	0.5664	0.5664	0.5664	0.5664
R_8	R_9	R_{10}	R_{11}	R_{12}	R_{13}	R_{14}
0.5664	0.5664	0.5664	10.9697	10.5639	10.1581	9.7524

Table 6.2: Mutual capacitances between adjacent coil domains. All capacitances are in Farads

C_1	C_2	C_3	C_4	C_5	C_6
4.15×10^{-11}	4.52×10^{-11}	4.52×10^{-11}	4.52×10^{-11}	4.52×10^{-11}	4.52×10^{-11}
C_7	C_8	C_9	C_{10}	C_{11}	C_{12}
4.52×10^{-11}	4.52×10^{-11}	4.52×10^{-11}	4.15×10^{-11}	1.58×10^{-9}	1.52×10^{-11}

C_{13}
$\times10^{-11}$

Table 6.3: Inductance matrix. All inductances are in represented in Henry units

L_{11}	L_{12}	L_{13}	L_{14}	L_{15}	L_{16}	L_{17}
2.82×10^{-5}	5.45×10^{-6}	1.92×10^{-6}	8.34×10^{-7}	4.17×10^{-7}	2.32×10^{-7}	1.39×10^{-7}
L_{18}	L_{19}	L_{110}	L_{111}	L_{112}	L_{113}	L_{114}
8.89×10^{-8}	5.95×10^{-8}	4.14×10^{-8}	4.53×10^{-5}	4.15×10^{-5}	3.81×10^{-5}	3.48×10^{-5}
L_{21}	L_{22}	L_{23}	L_{24}	L_{25}	L_{26}	L_{27}
5.45×10^{-5}	2.82×10^{-5}	5.45×10^{-6}	1.92×10^{-6}	8.34×10^{-7}	4.17×10^{-7}	2.32×10^{-7}
L_{28}	L_{29}	L_{210}	L_{211}	L_{212}	L_{213}	L_{214}
1.39×10^{-7}	8.89×10^{-8}	5.96×10^{-8}	6.59×10^{-5}	6.09×10^{-5}	5.62×10^{-5}	5.16×10^{-5}
L_{31}	L_{32}	L_{33}	L_{34}	L_{35}	L_{36}	L_{37}
1.92×10^{-6}	5.45×10^{-6}	2.82×10^{-5}	5.45×10^{-6}	1.92×10^{-6}	8.34×10^{-7}	4.17×10^{-7}

L_{38}	L_{39}	L_{310}	L_{311}	L_{312}	L_{313}	L_{314}
2.32×10^{-7}	1.39×10^{-7}	8.89×10^{-8}	7.16×10^{-5}	6.64×10^{-5}	6.13×10^{-5}	5.65×10^{-5}
L_{41}	L_{42}	L_{43}	L_{44}	L_{45}	L_{46}	L_{47}
8.34×10^{-7}	1.92×10^{-6}	5.45×10^{-6}	2.82×10^{-6}	5.45×10^{-6}	1.92×10^{-6}	8.34×10^{-7}
L_{48}	L_{49}	L_{410}	L_{411}	L_{412}	L_{413}	L_{414}
4.17×10^{-7}	2.32×10^{-7}	1.39×10^{-7}	7.38×10^{-5}	6.84×10^{-5}	6.32×10^{-5}	5.82×10^{-5}
L_{51}	L_{52}	L_{53}	L_{54}	L_{55}	L_{56}	L_{57}
4.17×10^{-7}	8.34×10^{-7}	1.92×10^{-6}	5.45×10^{-6}	2.82×10^{-5}	5.45×10^{-6}	1.92×10^{-6}
L_{58}	L_{59}	L_{510}	L_{511}	L_{512}	L_{513}	L_{514}
8.34×10^{-7}	4.17×10^{-7}	2.32×10^{-7}	7.45×10^{-5}	6.91×10^{-5}	6.39×10^{-5}	5.89×10^{-5}
L_{61}	L_{62}	L_{63}	L_{64}	L_{65}	L_{66}	L_{67}
2.32×10^{-7}	4.17×10^{-7}	8.34×10^{-7}	1.92×10^{-6}	5.45×10^{-6}	2.82×10^{-5}	5.45×10^{-6}
L_{68}	L_{69}	L_{610}	L_{611}	L_{612}	L_{613}	L_{614}
1.92×10^{-6}	8.34×10^{-7}	4.17×10^{-7}	7.45×10^{-5}	6.91×10^{-5}	6.39×10^{-5}	5.89×10^{-5}
L_{71}	L_{72}	L_{73}	L_{74}	L_{75}	L_{76}	L_{77}
1.39×10^{-7}	2.32×10^{-7}	4.17×10^{-7}	8.34×10^{-7}	1.92×10^{-6}	5.45×10^{-6}	2.82×10^{-5}
L_{78}	L_{79}	L_{710}	L_{711}	L_{712}	L_{713}	L_{714}
5.45×10^{-6}	1.92×10^{-6}	8.34×10^{-7}	7.38×10^{-5}	6.84×10^{-5}	6.32×10^{-5}	5.82×10^{-5}
L_{81}	L_{82}	L_{83}	L_{84}	L_{85}	L_{86}	L_{87}
8.89×10^{-8}	1.39×10^{-7}	2.32×10^{-7}	4.17×10^{-7}	8.34×10^{-7}	1.92×10^{-6}	5.45×10^{-6}
L_{88}	L_{89}	L_{810}	L_{811}	L_{812}	L_{813}	L_{814}
2.82×10^{-5}	5.45×10^{-6}	1.92×10^{-6}	7.16×10^{-5}	6.64×10^{-5}	6.13×10^{-5}	5.65×10^{-5}
L_{91}	L_{92}	L_{93}	L_{94}	L_{95}	L_{96}	L_{97}
5.95×10^{-8}	8.89×10^{-8}	1.39×10^{-7}	2.32×10^{-7}	4.17×10^{-7}	8.34×10^{-7}	1.92×10^{-6}
L_{98}	L_{99}	L_{910}	L_{911}	L_{912}	L_{913}	L_{914}
5.45×10^{-6}	2.82×10^{-5}	5.45×10^{-6}	6.59×10^{-5}	6.09×10^{-5}	5.62×10^{-5}	5.16×10^{-5}
L_{101}	L_{102}	L_{103}	L_{104}	L_{105}	L_{106}	L_{107}
4.14×10^{-8}	5.96×10^{-8}	8.89×10^{-8}	1.39×10^{-7}	2.32×10^{-7}	4.17×10^{-7}	8.34×10^{-7}
L_{108}	L_{109}	L_{1010}	L_{1011}	L_{1012}	L_{1013}	L_{1014}
1.92×10^{-6}	5.45×10^{-6}	2.82×10^{-5}	4.53×10^{-5}	4.15×10^{-5}	3.81×10^{-5}	3.48×10^{-5}
L_{111}	L_{112}	L_{113}	L_{114}	L_{115}	L_{116}	L_{117}
4.53×10^{-5}	6.59×10^{-5}	7.16×10^{-5}	7.38×10^{-5}	7.45×10^{-5}	7.45×10^{-5}	7.38×10^{-5}

L_{118}	L_{119}	L_{1110}	L_{1111}	L_{1112}	L_{1113}	L_{1114}
7.16×10^{-5}	6.59×10^{-5}	4.53×10^{-5}	0.00139	0.0013	0.00119	0.00110
L_{121}	L_{122}	L_{123}	L_{124}	L_{125}	L_{126}	L_{127}
4.15×10^{-5}	6.09×10^{-5}	6.64×10^{-5}	6.84×10^{-5}	6.91×10^{-5}	6.91×10^{-5}	6.84×10^{-5}
L_{128}	L_{129}	L_{1210}	L_{1211}	L_{1212}	L_{1213}	L_{1214}
6.64×10^{-5}	6.09×10^{-5}	4.15×10^{-5}	0.0013	0.00129	0.0012	0.00111
L_{131}	L_{132}	L_{133}	L_{134}	L_{135}	L_{136}	L_{137}
3.81×10^{-5}	5.62×10^{-5}	6.13×10^{-5}	6.32×10^{-5}	6.39×10^{-5}	6.39×10^{-5}	6.32×10^{-5}
L_{138}	L_{139}	L_{1310}	L_{1311}	L_{1312}	L_{1313}	L_{1314}
6.13×10^{-5}	5.62×10^{-5}	3.81×10^{-5}	0.001196	0.0012	0.00120	0.00111
L_{141}	L_{142}	L_{143}	L_{144}	L_{145}	L_{146}	L_{147}
3.48×10^{-5}	5.16×10^{-5}	5.65×10^{-5}	5.82×10^{-5}	5.89×10^{-5}	5.89×10^{-5}	5.82×10^{-5}
L_{148}	L_{149}	L_{1410}	L_{1411}	L_{1412}	L_{1413}	L_{1414}
5.65×10^{-5}	5.16×10^{-5}	3.48×10^{-5}	0.00110	0.00111	0.00111	0.00111

6.3.2 Electric Field and Potential Distribution Results and Discussion

Figure 6.3 shows the potential distribution at specific nodes as a function of frequency. Complete results are shown in Table 6.4. The equivalent circuit of coil sample is energized over a frequency range of 60 Hz to 20 kHz, and the node potentials are calculated respectively by solving the system of first order ODEs as described in Section 6.1.2. MATLAB™ ODE45 solver is used to solve the system of linear ordinary differential equations. The ODE45 solver is based on the Runga–Kutta 45 numerical algorithm. It is a one step solver which means in order to calculate any solution Y(tn), it requires immediately preceding solution Y(tn-1). ODE45 is used for non-stiff problem types. The solver integrates the system of differential equations from time t to t_f with initial conditions defined in a separate vector y_0.

Initially, the coil excitation voltage is kept constant at 5kV rms (7071 peak), which is the nominal voltage of the coil. Results in Fig 6.3 show that the node potentials drop drastically at higher frequencies. This change in potential distribution enhances the electrical stress between 4^{th} and 5^{th} winding layers at higher frequencies as shown in Fig 6.4, which shows a

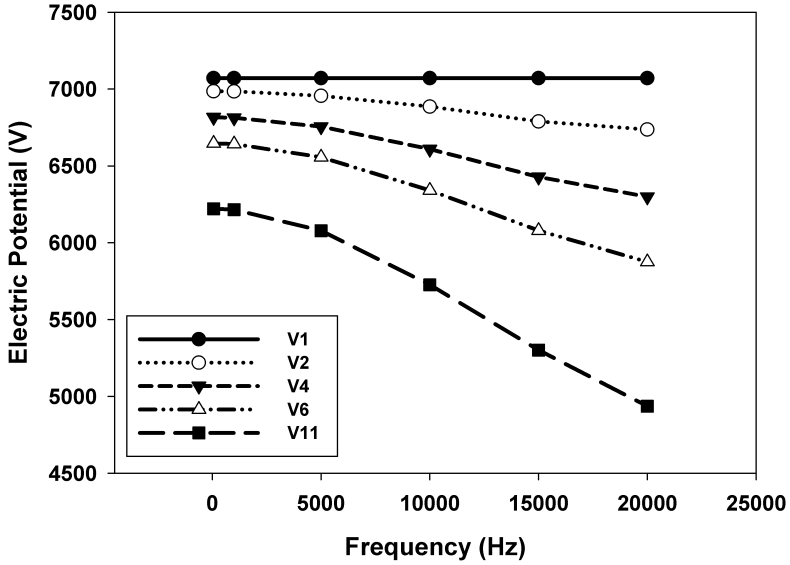

Figure 6.3: The potential distribution at various nodes as a function of frequency

Table 6.4: Node potentials as a function of frequency. All potentials are peak values presented as volts

Node	60Hz	1kHz	5kHz	10kHz	15kHz	20kHz
1	7071	7071	7071	7071	7071	7071
2	6986	6985	6956	6886	6789	6737
3	6901	6900	6867	6786	6679	6619
4	6816	6813	6755	6609	6428	6299
5	6730	6728	6666	6509	6318	6182
6	6646	6642	6556	6340	6079	5875
7	6560	6557	6467	6242	5970	5758
8	6475	6471	6361	6082	5746	5470
9	6390	6386	6272	5983	5635	5350
10	6305	6300	6170	5838	5436	5095
11	6221	6215	6078	5726	5301	4936
12	4574	4568	4422	4039	3569	3119
13	2988	2986	2922	2760	2565	2398
14	1463	1462	1414	1287	1128	975

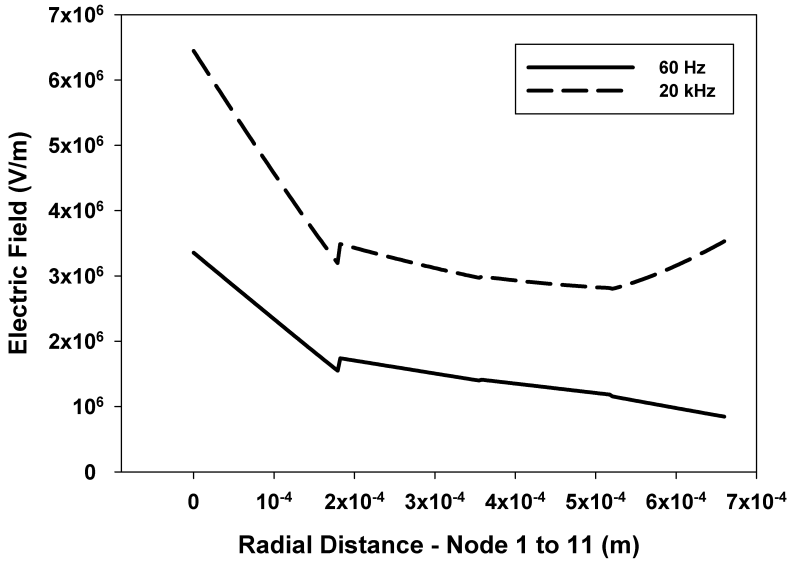

Figure 6.4: The electric field as a function of radial distance from node 1 and 11. The kink in the middle of the curve is due to the meshing

significantly enhanced electric field between 4^{th} and 5^{th} layer at higher frequencies; almost two times at 20 kHz as compared to 60 Hz. The node potentials are then calculated using various high frequency superimposed waveforms. A sample waveform is shown in Fig. 6.5. To see only the frequency effect in the simulated potential/field distribution, the peak voltage is kept constant at 7071 V peak for all the waveforms. Thus, the results can be compared with the clean 60 Hz, 5kV rms waveform. The superposition frequency is varied from 60 Hz to 20 kHz and the harmonic distortion level is kept constant at 25%. The results at different frequencies are shown in Fig. 6.6.

As expected, the node voltage drops at higher frequencies at a faster rate compared to that for 60 Hz, as we move away from the line end. It is also clear that the highest voltage drop occurred at node 11, which in our case is the 4^{th} layer of winding. This means the potential difference between the 4^{th} and 5^{th} layer increased significantly, thereby enhancing the electric field, which may exceed the threshold for any partial discharge (PD) activities.

The computed fields from the potentials are shown in Fig. 6.7. Despite keeping the peak values of the applied voltage, for 60 Hz and (60 Hz + 20 kHz) the same, the electric field is

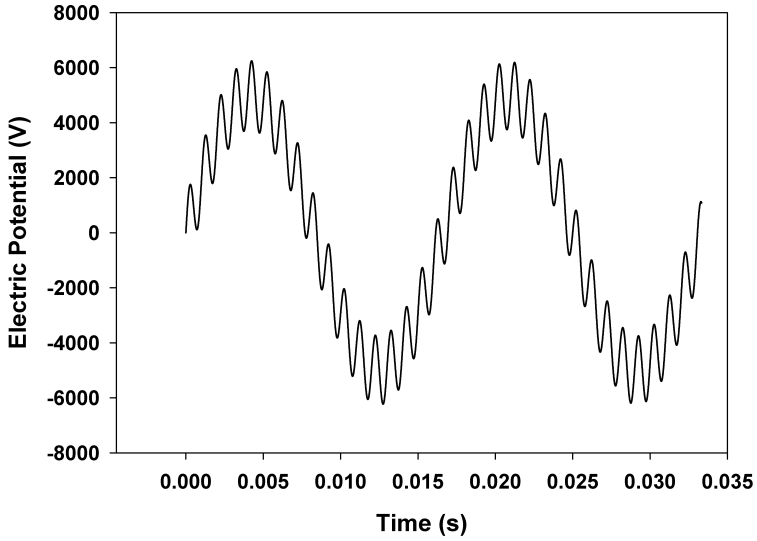

Figure 6.5: A typical voltage waveform with a 1 kHz signal superimposed on a 60 Hz sinusoid

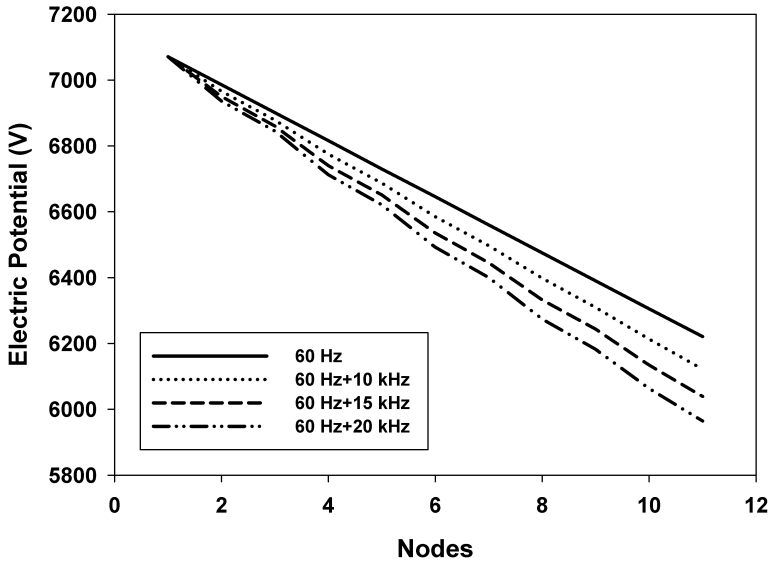

Figure 6.6: Node voltages at different frequencies superimposed on 60Hz. THD is maintained at 25%

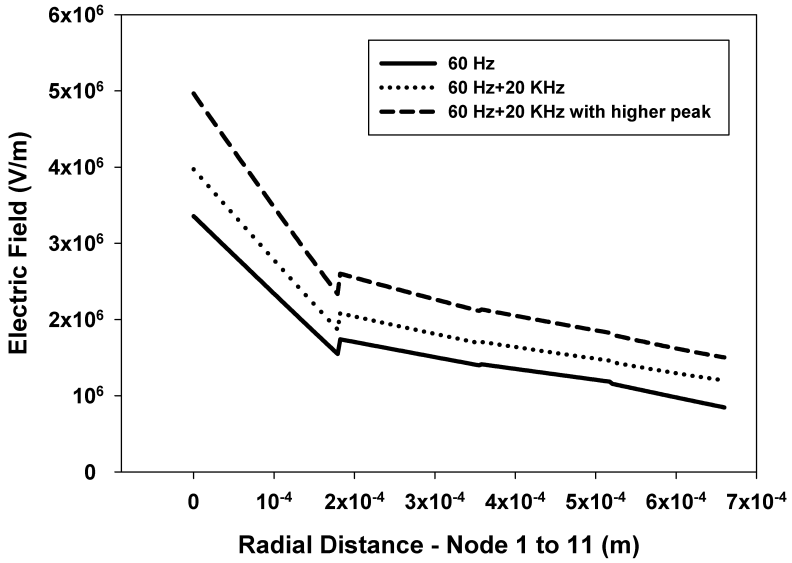

Figure 6.7: electric field as a function of the radial distance from node 1 and 11

always higher with voltage waveforms injected with high frequency harmonics. In practice, the situations can be even more severe as the injected harmonics are superimposed on top of the fundamental voltage. This effect is shown by computing the fields using higher peak, as shown in Fig 6.7. Any localized electric field enhancements will increase the PD activity in the region, and increase the aging rate of the insulation; hence reducing the operating life of the transformers.

6.4 Transformer Paper Insulation Aging Test Setup

Having identified the electric field redistribution in transformer and localized field enhancements due to high frequency, it is important to understand how it will impact on the transformer insulation system. To accomplish this goal a high frequency aging setup was designed to test the transformer paper insulation under clean and distorted waveforms. The schematic representation of test setup is shown in Fig 6.8

A unique approach is adopted to generate distorted waveforms. Instead of using a superposition circuit, the desired waveform was generated in computer through a MATLAB^{TM}

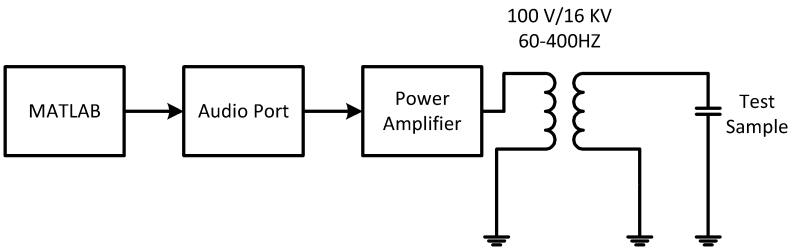

Figure 6.8: Schematic representation of high frequency test setup

based software and passed on to the audio port. The audio signal is then fed to a power amplifier to get the required amplification to be fed to a testing transformer. This approach is advantageous in a way that it can precisely control the required level of distortion in the output waveform. With this approach, the following four parameters of the waveform can be adjusted accurately:

1. Peak value
2. Frequency
3. DC offset
4. Phase shift

However, it is limited by the frequency response of the testing transformer. With test transformer components used in this work, it is possible to generate up to 400 Hz voltage signals.

Test samples are prepared from thermally upgraded paper insulation extracted from a disconnected real-time transformer winding section. The samples are made by wrapping the paper insulation on small copper windings. Electrical stress is applied to the samples installed in oil-filled cell. The oil used is new Naphthenic oil. Figure 6.9 depicts the paper samples along with the oil-filled cell used in the experiment.

Accelerated aging experiments on transformer paper insulation are performed through three test protocols: A, B and C as summarized in Table 6.5. Each protocol has a different applied voltage waveform. In protocol A, the voltage waveform applied is a 14kV pk-pk sinusoidal voltage waveform with a spectrum composed of the fundamental frequency (60

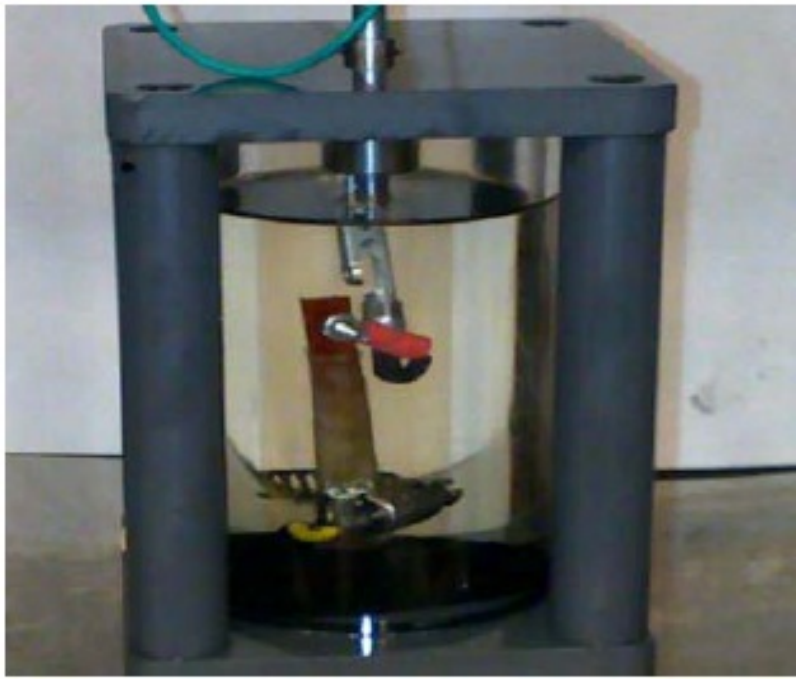

Figure 6.9: Transformer paper insulation test sample

Hz) component only. In protocols B and C, the applied test voltage waveforms have a total harmonic distortion (THD) of 14% and 28% respectively. Such high levels of distortions are chosen in order to accelerate the aging process. The harmonic components included

Table 6.5: Test protocols applied in the accelerated ageing experiments

Protocol	Frequency spectrum of the applied voltage waveform	Remarks
A	14 kV pk-pk 60Hz + 0% THD	Sample 1 and 2 are tested
B	14 kV pk-pk 60Hz + 14% THD (500 V 3^{rd} and 5^{th} harmonics)	Sample 3 is tested
C	14 kV pk-pk 60Hz + 28% THD (1 kV 3^{rd} and 5^{th} harmonics)	Sample 4 and 5 are tested (Sample 5 is failed during aging test)

in protocol B are the 3^{rd} and 5^{th} order harmonics with a level of 500V. The harmonic components included in protocol C are also the 3rd and 5th order harmonics, but with a level of 1kV. Samples 1 and 2 are tested using protocol A. Sample 3 is tested using protocol

B. Samples 4 and 5 are tested using protocol C. Other low order harmonics, like the 7^{th} and the 11^{th}, are not considered in this study due to the limitation of the operational frequency of the transformer used in the experiment (400 Hz). Figures 6.10–6.12 show the applied voltage waveforms in the three designed protocols (A, B and C).

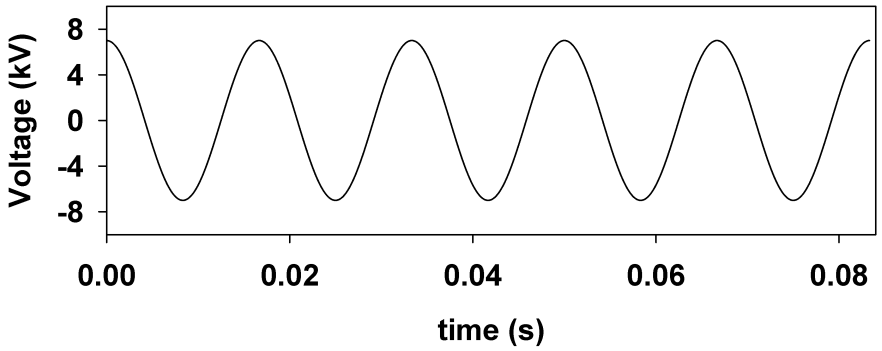

Figure 6.10: Voltage waveform applied in protocol A; composed of a 60 Hz fundamental + 0% THD.

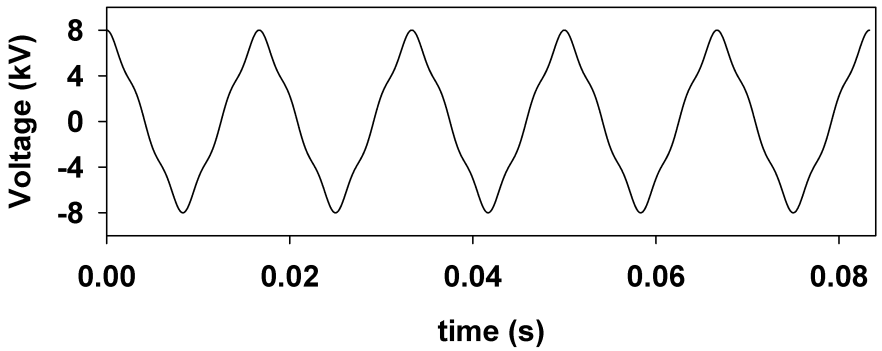

Figure 6.11: Voltage waveform applied in protocol B; composed of a 60 Hz fundamental + 14% THD.

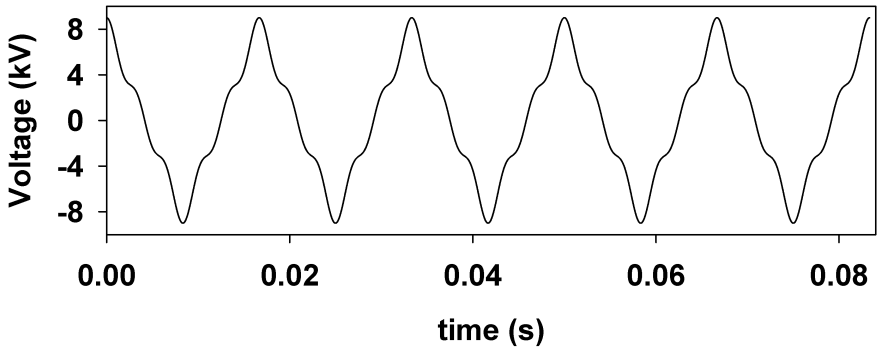

Figure 6.12: Voltage waveform applied in protocol C; composed of a 60 Hz fundamental + 28% THD.

6.5 Transformer Paper Insulation Aging Results and Discussion

This section presents the results of the aging experiment developed to understand the effects of high frequency distortions on transformer paper insulation. Dissipation factor measurements are used as a comparison tool to assess the insulation condition before and after aging, because dissipation factor test on older apparatus provides information regarding the general condition and aging of the insulation [96]. Table 6.6 shows the measured dissipation factors of the paper samples before and after aging tests, under different electrical stresses. The data presented are the average values from nine different measurements. The aging test duration is 72 hours. The levels of THD chosen are higher than those values reported by R. K. Varma et al. [2] in order to accelerate the aging process. According to IEEE PC57.152, a meaningful evaluation of DF will include comparison to previous test results [96]. The ratio of the increment in the dissipation factor or dielectric loss is used as criteria for comparing the aged samples under the three different protocols (A, B and C). The dissipation factor increment ratio (DFIR) is calculated as in (6.19):

$$DFIR = \frac{DF_{afteraging}}{DF_{beforeaging}} \tag{6.19}$$

Table 6.6: Dissipation factor measurements conducted on samples before and after aging for the samples identified in the protocols: A, B and C.

DF measurement frequency	Average DF before aging	Average DF after aging		
		60 Hz+0% THD (A)	60 Hz+14% THD (B)	60 Hz+28% THD (C)
60 Hz	0.013	0.013	0.019	0.025
400 Hz	0.006	0.006	0.01	0.012
1 kHz	0.004	0.006	0.007	0.009

Figure 6.13 depicts the DFIR measured using three DF source frequencies (60Hz, 400Hz, and 1 kHz). For the samples tested under protocol A, no significant change in the dissipation factor has been detected. On the other hand, a considerable change in the dissipation factor has been found when the paper insulation is stressed as per protocols B and C. The minimum DFIR for DF measurement frequency of 400Hz is increased by 50%. When the

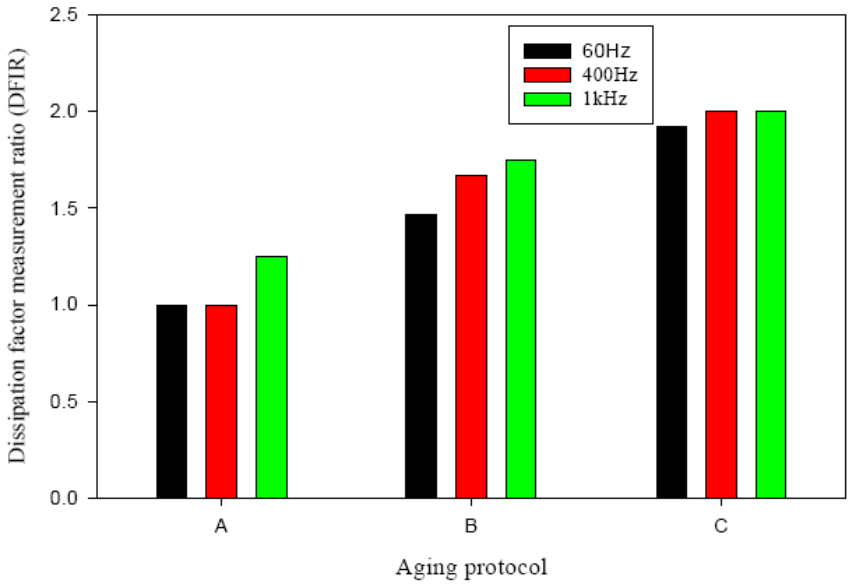

Figure 6.13: A comparison of the dissipation factor increment ratio (DFIR) for the three test protocols (A, B and C).

THD of the applied voltage waveform is increased in protocol C, the DFIR has increased more than that tested under protocol B. It can be concluded that the aging has been increased by a factor of 2 when the THD of a distorted voltage waveform with the 3^{rd} and 5^{th} harmonic is 28%. It has been found in [97] that the aging rate or the failure rate is increased by 2 when paper insulation samples are stressed using distorted voltage waveform with high-frequency harmonics. Our results show that the effects due to low-order harmonics are as significant as those found with high-order harmonics [97].

It is evident from Fig 6.13 that the change in DFIR is more sensitive to the change of the measured sample when the DF source frequencies are 60 and 400Hz. The sensitivity is very low for the DFIR to change with the aged sample at 1 kHz DF source frequency. At low frequencies, the effect of interfacial polarization on DF measurement should be dominant. Accordingly, it can be inferred that the aging process is localized on the interfacial points in the tested samples. The failure in one of the samples tested under protocol C gives an indication of the probability of occurrence of breakdown due to severe degradation in the paper insulation samples. However, additional aging experiments are needed to verify the significance of degradation on insulation breakdown. Moreover, other analytical tests like degree of polymerization and tensile strength are helpful to assess the type and level of insulation degradation.

Chapter 7

Summary, Conclusions and Future Work

7.1 Summary and Conclusions

The objective of this study was to demonstrate the deteriorative effects of high frequency on transformer insulation. For this reason the winding system was thoroughly analysed, both in simulations and in experiments.

The opening chapter reviewed Ontario's energy sources, wind and solar technologies and their concentration in Ontario's grid. It also discussed the presence of harmonics in the distribution system, voltage source converter technologies and the knowledge available about their impact on various insulation systems such as machine insulation and cable terminations. An overview of the transformer insulation system and the high frequency high voltage generation methods were also presented. Following this, the modeling procedure of a test distribution feeder, design of a partial discharge localization experiment, design of a high voltage air core coil and its finite element model representation were discussed. Also, the design of high frequency aging experiment was presented. A base case for thesis was developed by identifying the harmonic resonance problem in a DG loaded distribution feeder. Having identified the problem, a partial discharge localization experiment was performed on a dry-type transformer. The objective of this experiment was to identify the dependence of field distribution on frequency. If the electric field distribution changes at

higher frequency then electric field concentration will develop at a different location in the transformer winding; hence, it creates a different location of partial discharge. A detailed electric field simulation study was carried out on a high voltage air core coil after it was identified from partial discharge localization experiment that field distribution is different at higher frequencies. Lastly, an aging study was carried out on a paper insulation sample from a field aged transformer. Paper samples were aged under power frequency and distorted waveforms with various total harmonic distortion levels. Dissipation factor was used as a comparison factor for aged and un-aged samples.

From the work done in this thesis, following conclusions can be drawn:

1. Distribution feeders loaded with high density of dispersed generation units are susceptible to high frequency distortion. The presence of DGs in the feeder makes the feeder resonance floating; hence it is no more a deterministic value. Therefore, it is difficult to design proper filters. In this situation the high frequency impact on the transformer insulation needs to be understood thoroughly so as to make appropriate design changes, as transformers are the most vital and expensive component of power system.

2. The high frequency aging experiment showed a significant rise in dissipation factor of paper insulation compared to power frequency aging. A higher rise in dissipation factor implies faster insulation degradation. Early transformer failure is not only a reliability issue, it also means a loss of asset which directly translates to financial loss due to equipment cost and also due to down time losses.

3. It has been shown that finite element software can be used to understand the behaviour of electric field distribution at higher frequencies. Electric field concentration spots can be identified at an acceptable accuracy.

4. It has been demonstrated that AE technique can be successfully utilized together with the acoustic waveguide to identify the electric field concentration areas in the transformer winding by locating partial discharge in the winding.

5. High frequency application changes the field distribution in the winding, and it may cause field enhancements which may lead to partial discharges in the winding. Partial discharges are one of the aging mechanisms of insulation degradation. High

frequency induced partial discharges may increase the aging rate of the insulation; hence, causing faster degradation.

6. High frequency stresses also induce dielectric heating which is another insulation degradation mechanism. The dissipation factor (DF) of paper insulation increases due to dielectric heating. DF of high frequency aged paper samples increased twice compared to paper samples aged under power frequency.

7.2 Propositions for Future Work

Due to little amount of knowledge in the area of high frequency effects on transformer insulation it is important to take this study further to a next level. For this reason, this section will give suggestions for future work which can be done in this area to increase the knowledge base about the subject.

To completely understand the effects of high frequency on a transformer insulation system, long term aging tests are suggested. To imitate the real conditions it is suggested that at least a two week continuous power quality data is collected from the point of common coupling. Statistical analysis should be done on the collected data to identify which harmonics are critical, distortion levels, frequency of occurrence of capacitor bank switching transients etc and similar kind of waveforms should be used for long term aging experiments. Also, in real conditions, transformers are subjected to loading cycles which correspond to a temperature cycle. Therefore to make the tests more realistic, temperature cycles should be introduced during aging experiments. It will be interesting to compare the performance of normal Kraft paper and thermally upgraded paper under high frequency stresses, and if required, then proper stress grading material should be designed and introduced in the high stress areas within the transformer winding.

Experimental setup should be improved in terms of power and frequency. This can be done using a Tesla transformer which was successfully implemented by the researchers [69, 78]. If the generator can generate very high frequencies, above 20 kHz, then it can help improving the aging setup such that high frequency waveforms not only imitate the high frequency switching harmonics generated by the power converters but also help accelerate the aging process; hence reduce time for aging experiment.

An understanding of electric field distribution inside the transformer winding is developed in this thesis. In order to improve the finite element model, it is primal to calculate the conductivity and permittivity of transformer insulation system and to develop an understanding of frequency and temperature dependence of conductivity and permittivity of the insulation system. Guarded electrodes must be used for the measurement of material properties at higher frequency to avoid the stray capacitances.

Depending on the long term aging experiments, if required, better insulation materials or perhaps some stress grading should be developed in the lab, then introduced in transformer insulation system and tested against long term aging experiments. Finally, a field dependent material may improve the performance under high frequency field enhancement and capacitor switching transients which may be present due to frequent switching of power factor coupling capacitors at the terminals of wind turbine generators.

APPENDICES

Appendix A

IEEE 34 Bus Distribution Feeder Parameters

Overhead Line Configurations				
Config.	Phasing	Phase - ACSR	Neutral - ACSR	Spacing ID
300	BACN	1/0	1/0	500
301	BACN	#2 6/1	#2 6/1	500
302	AN	#4 6/1	#4 6/1	510
303	BN	#4 6/1	#4 6/1	510
304	BN	#2 6/1	#2 6/1	510

Line Segment Data			
Node A	Node B	Length(ft.)	Config.
800	802	2580	300
802	806	1730	300
806	808	32230	300
808	810	5804	303
808	812	37500	300
812	814	29730	300

Line Segment Data			
Node A	Node B	Length(ft.)	Config.
814	850	10	301
816	818	1710	302
816	824	10210	301
818	820	48150	302
820	822	13740	302
824	826	3030	303
824	828	840	301
828	830	20440	301
830	854	520	301
832	858	4900	301
832	888	0	XFM-1
834	860	2020	301
834	842	280	301
836	840	860	301
836	862	280	301
842	844	1350	301
844	846	3640	301
846	848	530	301
850	816	310	301
852	832	10	301
854	856	23330	303
854	852	36830	301
858	864	1620	302
858	834	5830	301
860	836	2680	301
862	838	4860	304
888	890	10560	300

Transformer Data					
	kVA	kV-high	kV-low	R-%	X-%
Substation:	2500	69 - D	24.9 -Gr. W	1	8
XFM -1	500	24.9 - Gr.W	4.16 - Gr. W	1.9	4.08

Spot Loads							
Node	Load Model	Ph-1 kW	Ph-1 kVAr	Ph-2 kW	Ph-2 kVAr	Ph-3 kW	Ph-4 kVAr
860	Y-PQ	20	16	20	16	20	16
840	Y-I	9	7	9	7	9	7
844	Y-Z	135	105	135	105	135	105
848	D-PQ	20	16	20	16	20	16
890	D-I	150	75	150	75	150	75
830	D-Z7	10	5	10	5	25	10
Total		344	224	344	224	359	229

Distributed Loads								
Node A	Node B	Load Model	Ph-1 kW	Ph-1 kVAr	Ph-2 kW	Ph-2 kVAr	Ph-3 kW	Ph-3 kVAr
802	806	Y-PQ	0	0	30	15	25	14
808	810	Y-I	0	0	16	8	0	0
818	820	Y-Z	34	17	0	0	0	0
820	822	Y-PQ	135	70	0	0	0	0
816	824	D-I	0	0	5	2	0	0
824	826	Y-I	0	0	40	20	0	0
824	828	Y-PQ	0	0	0	0	4	2
828	830	Y-PQ	7	3	0	0	0	0
854	856	Y-PQ	0	0	4	2	0	0
832	858	D-Z	7	3	2	1	6	3

Distributed Loads								
Node A	Node B	Load Model	Ph-1 kW	Ph-1 kVAr	Ph-2 kW	Ph-2 kVAr	Ph-3 kW	Ph-3 kVAr
858	864	Y-PQ	2	1	0	0	0	0
858	834	D-PQ	4	2	15	8	13	7
834	860	D-Z	16	8	20	10	110	55
860	836	D-PQ	30	15	10	6	42	22
836	840	D-I	18	9	22	11	0	0
862	838	Y-PQ	0	0	28	14	0	0
842	844	Y-PQ	9	5	0	0	0	0
844	846	Y-PQ	0	0	25	12	20	11
846	848	Y-PQ	0	0	23	11	0	0
Total			262	133	240	120	220	114

Shunt Capacitors			
Node	Ph-A kVAr	Ph-B kVAr	Ph-C kVAr
844	100	100	100
848	150	150	150
Total	250	250	250

Appendix B

High Voltage Coil Design Parameters

5 kV HV coil 75 kV BIL		
Winding	**HV**	**~**
Coils	1	0
Form	1.75"x0.625"	
Insulation		Over HV **8** - *4 mil* Pucaro **1** *1mm press board*
Conductor	1-#30 Cu	
Size Inusl.	0.012x0.012	~
Stay Back	0.500"	~
Turns	1667	
Turns/layer	371	~
Layers	5	
Layer Insulation	1 - 4mil Pucaro	
	2 - 7 mil Pucaro	~ ~
	Note Extra Paper: 2 - 4mil Pucaro btwn 4-5	

Bibliography

[1] http://www.oe.energy.gov/smartgrid.htm. 1

[2] D. Patel, R. Varma, R. Seethapathy, and M. Dang, "Impact of wind turbine generators on network resonance and harmonic distortion," in *Electrical and Computer Engineering (CCECE), 2010 23rd Canadian Conference on*, pp. 1 –6, may 2010. 2, 24, 25, 38, 70

[3] "Public utility holding company act of 1935 : 1935-1992," January 1993. 2

[4] http://en.wikipedia.org/wiki/Federal_Power_Act. 2

[5] http://en.wikipedia.org/wiki/EPA. 2

[6] http://en.wikipedia.org/wiki/PURPA. 2

[7] http://thomas.loc.gov/cgi-bin/query/z?c102:H.R.776.ENR:. 3

[8] http://www.ferc.gov/legal/maj-ord-reg/land-docs/2000a.pdf. 3

[9] http://www.ferc.gov/legal/maj-ord-reg/land-docs/rm95-8-00w.txt. 3

[10] D. Bradley, "Renewable Portfolio Standards (RPS) and Other Incentives Harmonization Opportunities in Canada," February 2005. 3

[11] http://fit.powerauthority.on.ca/what-feed-tariff-program. 3

[12] http://www.ontla.on.ca/web/bills/bills_detail.do?locale=en&BillID=2145. 3

[13] http://www.queensu.ca/qieep/files/presentations/Distributed_Generation/DISTGEN_1_2_Toneguzzo.pdf. 4

[14] "Impact of Increasing Contribution of Dispersed Generation on the Power System," 1998. 4

[15] P. Dondi, D. Bayoumi, C. Haederli, D. Julian, and M. Suter, "Network integration of distributed power generation," *Journal of Power Sources*, vol. 106, no. 1-2, pp. 1 – 9, 2002. 4

[16] G. Pepermans, J. Driesen, D. Haeseldonckx, R. Belmans, and W. D'haeseleer, "Distributed generation: definition, benefits and issues," *Energy Policy*, vol. 33, no. 6, pp. 787 – 798, 2005. 4

[17] S. J. M. J. A. J. J, "Impact of Distributed Generation on Voltage Stability: a Review." 4

[18] http://www.cleantechsandiego.org/reports/ImpactsofDistributedGenerationReport_2010.pdf. 4

[19] T. Ackermann, G. Andersson, and L. Sder, "Distributed generation: a definition," *Electric Power Systems Research*, vol. 57, no. 3, pp. 195 – 204, 2001. 4

[20] W. El-Khattam and M. M. A. Salama, "Distributed generation technologies, definitions and benefits," *Electric Power Systems Research*, vol. 71, no. 2, pp. 119 – 128, 2004. 5

[21] http://www.mei.gov.on.ca/en/pdf/MEI_LTEP_en.pdf. 6, 9

[22] http://www.ieso.ca/imoweb/pubs/marketReports/18MonthOutlook_2006dec.pdf. 6

[23] http://www.ieso.ca/imoweb/media/md_supply.asp. 6

[24] http://ebridge.enbridge.com/eBridge/volume62/article1.php. 6, 13

[25] http://documents.rec.org/topic-areas/REN21_GSR_2010.pdf. 6, 7, 8

[26] H. Polinder, F. van der Pijl, G.-J. de Vilder, and P. Tavner, "Comparison of direct-drive and geared generator concepts for wind turbines," *Energy Conversion, IEEE Transactions on*, vol. 21, pp. 725 –733, sept. 2006. 9

[27] Y. Duan and R. Harley, "Present and future trends in wind turbine generator designs," in *Power Electronics and Machines in Wind Applications, 2009. PEMWA 2009. IEEE*, pp. 1 –6, june 2009. 9, 10, 11, 12

[28] D. S. R. H. K. Mountawakkil and C. Saniter, "Power quality behavior of large wind parks with variable speed wind energy converter," in *17th International Conference on Electricity Distribution, paper No. 28, Barcelona*, May 2003. 9

[29] B. B. . K.B.Mohanty, "Doubly-fed induction generator for variable speed wind energy conversion systems- modeling & simulation," *International Journal of Computer and Electrical Engineering*, vol. 2, pp. 141–147, February 2010. 10

[30] C. Mozina, "Impact of wind power generation on distribution systems," in *Rural Electric Power Conference (REPC), 2010 IEEE*, pp. B5 –B5–7, may 2010. 10

[31] N. J. T. Burton, D. Sharpe and E. Bossanyi, *Wind Energy Handbook*. John Wiley & Sons, 2001. 12, 13

[32] `http://en.wikipedia.org/wiki/Solar_power`. 13

[33] `http://www.bmu.de/files/english/renewable_energy/downloads/application/pdf/broschuere_ee_zahlen_en.pdf`. 13

[34] W. C. Cooley, "Solar direct-conversion power systems," *Military Electronics, IRE Transactions on*, vol. MIL-6, pp. 91 –98, jan. 1962. 13

[35] E. van Voorthuysen, "The promising perspective of concentrating solar power (csp)," in *Future Power Systems, 2005 International Conference on*, pp. 7 pp. –7, nov. 2005. 13, 14

[36] A. G. Hoffmann, *Photovoltaic Solar Energy Generation*. Springer-Verlag Berlin Heidelberg 2005, 2005. 15

[37] F. Li, W. Li, F. Xue, Y. Fang, T. Shi, and L. Zhu, "Modeling and simulation of large-scale grid-connected photovoltaic system," in *Power System Technology (POWERCON), 2010 International Conference on*, pp. 1 –6, oct. 2010. 15, 17, 18

[38] D. P. Hodel, "Photovoltaics—electricity from sunlight." 15, 17

[39] H. Fernandez, A. Martinez, V. Guzman, and M. Gimenez, "A simple, low cost design using current feedback to improve the efficiency of a mppt-pv system for isolated locations," in *Power Electronics and Motion Control Conference, 2008. EPE-PEMC 2008. 13th*, pp. 1947 –1950, sept. 2008. 17

[40] R. Leyva, C. Alonso, I. Queinnec, A. Cid-Pastor, D. Lagrange, and L. Martinez-Salamero, "Mppt of photovoltaic systems using extremum - seeking control," *Aerospace and Electronic Systems, IEEE Transactions on*, vol. 42, pp. 249 – 258, jan. 2006. 17

[41] C. Cabal, C. Alonso, A. Cid-Pastor, B. Estibals, L. Seguier, R. Leyva, G. Schweitz, and J. Alzieu, "Adaptive digital mppt control for photovoltaic applications," in *Industrial Electronics, 2007. ISIE 2007. IEEE International Symposium on*, pp. 2414 –2419, june 2007. 17

[42] M. H. Rahsid, ed., *Power Electronics Handbook*. Academic Press, 2001. 20

[43] E. Muljadi, "Pv water pumping with a peak-power tracker using a simple six-step square-wave inverter," *Industry Applications, IEEE Transactions on*, vol. 33, pp. 714 –721, may/jun 1997. 20

[44] H. Kim, Y. Chung, K. Lee, Y. Jon, and K. Kim, "Performance analysis of soft-switching inverter for the photovoltaic power system," in *Power Electronics, 2007. ICPE '07. 7th Internatonal Conference on*, pp. 436 –439, oct. 2007. 20

[45] R. Nakagomi, Y. Zhao, and B. Lehman, "Multi-level converters for three-phase photovoltaic applications," in *Control and Modeling for Power Electronics (COMPEL), 2010 IEEE 12th Workshop on*, pp. 1 –6, june 2010. 20

[46] M. Honsberg and T. Radke, "3-level igbt modules with trench gate igbt and their thermal analysis in ups, pfc and pv operation modes," in *Power Electronics and Applications, 2009. EPE '09. 13th European Conference on*, pp. 1 –7, sept. 2009. 20

[47] L. Helle and S. Munk-Nielsen, "Comparison of converter efficiency in large variable speed wind turbines," in *Applied Power Electronics Conference and Exposition, 2001. APEC 2001. Sixteenth Annual IEEE*, vol. 1, pp. 628 –634 vol.1, 2001. 20

[48] K. Thorborg, *Power Electronics*. Prentice-Hall, 1988. 21, 22

[49] E. Ozdemir, S. Ozdemir, L. Tolbert, and B. Ozpineci, "Fundamental frequency modulated multilevel inverter for three-phase stand-alone photovoltaic application," in *Applied Power Electronics Conference and Exposition, 2008. APEC 2008. Twenty-Third Annual IEEE*, pp. 148 –153, feb. 2008. 21, 22

[50] "IEEE Recommended Practices and Requirements for Harmonic Control in Electrical Power Systems," *IEEE Std 519-1992*, 1993. 23

[51] `http://staff.bath.ac.uk/eesmm/Investigation%20of%20the%20Behaviour%20of%20Wind%20Turbines%20under%20Low%20Turbulence%20Wind%20Conditions%20and%20Their%20Interaction%20with%20the%20Distribution%20Grid.pdf`. 23

[52] G. Esposito, D. Zaninelli, G. Lazaroiu, and N. Golovanov, "Impact of embedded generation on the voltage quality of distribution networks," in *Electrical Power Quality and Utilisation, 2007. EPQU 2007. 9th International Conference on*, pp. 1 –6, oct. 2007. 23, 24

[53] "Electromagnetic compatibility (EMC) - Part 3-6: Limits - Assessment of emission limits for the connection of distorting installations to MV, HV and EHV power systems," February 2008. 23

[54] M. Bollen, L. Yao, S. Ro andnnberg, and M. Wahlberg, "Harmonic and interharmonic distortion due to a windpark," in *Power and Energy Society General Meeting, 2010 IEEE*, pp. 1–6, july 2010. 24

[55] J. Balcells and D. Gonzalez, "Harmonics due to resonance in a wind power plant," in *Harmonics And Quality of Power, 1998. Proceedings. 8th International Conference on*, vol. 2, pp. 896 –899 vol.2, oct 1998. 25, 26

[56] J. Li, N. Samaan, and S. Williams, "Modeling of large wind farm systems for dynamic and harmonics analysis," in *Transmission and Distribution Conference and Exposition, 2008. T x00026;D. IEEE/PES*, pp. 1 –7, april 2008. 25

[57] W. Wiechowski and P. Eriksen, "Selected studies on offshore wind farm cable connections - challenges and experience of the Danish TSO," in *Power and Energy Society General Meeting - Conversion and Delivery of Electrical Energy in the 21st Century, 2008 IEEE*, pp. 1 –8, july 2008. 25

[58] A. Bonnett, "Analysis of the impact of pulse-width modulated inverter voltage waveforms on ac induction motors," *Industry Applications, IEEE Transactions on*, vol. 32, pp. 386 –392, mar/apr 1996. 26

[59] J. Wheeler, "Effects of converter pulses on the electrical insulation in low and medium voltage motors," *Electrical Insulation Magazine, IEEE*, vol. 21, pp. 22 –29, march-april 2005. 26

[60] S. Haq, S. Jayaram, and E. Cherney, "Aging characterization of medium voltage groundwall insulation intended for pwm applications," in *Electrical Insulation, 2006. Conference Record of the 2006 IEEE International Symposium on*, pp. 143 –146, june 2006. 26

[61] F. Espino-Cortes, E. Cherney, and S. Jayaram, "Effectiveness of stress grading coatings on form wound stator coil groundwall insulation under fast rise time pulse voltages," *Energy Conversion, IEEE Transactions on*, vol. 20, pp. 844 – 851, dec. 2005. 26

[62] L. Ming, F. Sahlen, S. Halen, G. Brosig, and L. Palmqvist, "Impacts of high-frequency voltage on cable-terminations with resistive stressgrading," in *Solid Dielectrics, 2004. ICSD 2004. Proceedings of the 2004 IEEE International Conference on*, vol. 1, pp. 300 – 303 Vol.1, july 2004. 26

[63] S. H. G. B. L. Ming, F. Sahlen and L. Palmqvist, "Insulation Performance of Cable terminations with Resistive Stress-grading under High Frequency Voltages," in *XIVth International Symposium on High Voltage Engineering,Paper I-18*, pp. 1–4, 2005. 26

[64] F. Espino-Cortes, S. Jayaram, and E. Cherney, "Stress grading materials for cable terminations under fast-rise time pulses," *Dielectrics and Electrical Insulation, IEEE Transactions on*, vol. 13, pp. 430 –435, april 2006. 26

[65] T. Koltunowicz, G. Bajracharya, D. Djairam, and J. Smit, "Investigating the effects of repetitive transients on paper insulation," in *Developments in Power System Protection (DPSP 2010). Managing the Change, 10th IET International Conference on*, pp. 1 –5, 29 2010-april 1 2010. 27, 31

[66] "ANSI/NEMA MW 1000-2008 Revision 2-2010, *Magnet Wire*," September 2010. 27

[67] S. Grzybowski, A. Mani, and C. Taylor, "Partial discharge patterns of magnet wire samples under voltage stresses," in *Electrical Insulation and Dielectric Phenomena, 2005. CEIDP '05. 2005 Annual Report Conference on*, pp. 422 – 425, oct. 2005. 27

[68] B. Sonerud, T. Bengtsson, J. Blennow, and S. Gubanski, "Dielectric heating in insulating materials subjected to voltage waveforms with high harmonic content," *Dielectrics and Electrical Insulation, IEEE Transactions on*, vol. 16, pp. 926 –933, august 2009. 27

[69] L. Paulsson, B. Ekehov, S. Halen, T. Larsson, L. Palmqvist, A.-A. Edris, D. Kidd, A. Keri, and B. Mehraban, "High-frequency impacts in a converter-based back-to-back tie; the eagle pass installation," *Power Delivery, IEEE Transactions on*, vol. 18, pp. 1410 – 1415, oct. 2003. 27, 36, 75

[70] A. Elmoudi, M. Lehtonen, and H. Nordman, "Effect of harmonics on transformers loss of life," in *Electrical Insulation, 2006. Conference Record of the 2006 IEEE International Symposium on*, pp. 408 –411, june 2006. 27

[71] S. Sadati, A. Tahani, M. Jafari, and M. Dargahi, "Derating of transformers under non-sinusoidal loads," in *Optimization of Electrical and Electronic Equipment, 2008. OPTIM 2008. 11th International Conference on*, pp. 263 –268, may 2008. 27

[72] M. Nagel and T. Leibfried, "Investigation on the high frequency, high voltage insulation properties of mineral transformer-oil," in *Electrical Insulation and Dielectric Phenomena, 2006 IEEE Conference on*, pp. 226 –228, oct. 2006. 28

[73] T. Saha, "Review of modern diagnostic techniques for assessing insulation condition in aged transformers," *Dielectrics and Electrical Insulation, IEEE Transactions on*, vol. 10, pp. 903 – 917, oct. 2003. 30, 31

[74] M. J. Heathcote, *The J & P Transformer Book*. Newnes, 13$^{\text{th}}$ ed., 2007. 30, 32, 33, 34, 57

[75] D. Shroff and A. Stannett, "A review of paper aging in power transformers," *Generation, Transmission and Distribution, IEE Proceedings C*, vol. 132, pp. 312 –319, november 1985. 31, 32

[76] C. A. Bozzini, "Transformer Ageing Diagnosis by Means of Measurements of the Degree of Polymerization Results of New Experiments," in *CIGRE, Paper No. 12-08,Paris, France*, 1968. 31

[77] E. S. W. Lampe and K. Carrander, "Continuous Purification and Supervision of Transformer Insulation System in Service," in *IEEE Winter Power Meeting*, pp. 111–117, 1978. 31

[78] M. Nagel, C. Herold, T. Wenzel, and T. Leibfried, "Combined high frequency and high voltage insulation system investigation," in *Electrical Insulation, 2006. Conference Record of the 2006 IEEE International Symposium on*, pp. 440 –443, june 2006. 34, 75

[79] N. Hardt and D. Koenig, "Testing of insulating materials at high frequencies and high voltage based on the tesla transformer principle," in *Electrical Insulation, 1998. Conference Record of the 1998 IEEE International Symposium on*, vol. 2, pp. 517 –520 vol.2, jun 1998. 34, 35

[80] M. S. Naidu, *High Voltage Engineering*. McGraw-Hill, 1995. 35

[81] F. Guastavino, L. Centurioni, A. Dardano, and E. Torello, "Electrical treeing inception and growth in xlpe in presence of harmonics," in *Solid Dielectrics, 2004. ICSD 2004.*

Proceedings of the 2004 IEEE International Conference on, vol. 1, pp. 363 – 366 Vol.1, july 2004. 36

[82] G. Montanari and D. Fabiani, "The effect of nonsinusoidal voltage on intrinsic aging of cable and capacitor insulating materials," *Dielectrics and Electrical Insulation, IEEE Transactions on*, vol. 6, pp. 798 –802, dec 1999. 36

[83] H. Suzuki, Y. Ohki, Y. Nakamichi, and K. Ajiki, "Water tree characteristics in low-density polyethylene under power-frequency voltages with high-frequency components," in *Electrical Insulation and Dielectric Phenomena, 1996. IEEE 1996 Annual Report of the Conference on*, vol. 2, pp. 742 –745 vol.2, oct 1996. 36

[84] `http://ewh.ieee.org/soc/pes/dsacom/testfeeders/index.html`. 38, 39

[85] S. Heier, *Grid Integration of Wind Energy Conversion Systems*. John Wiley & Sons, Ltd, 2004. 38

[86] R. Zavadil, N. Miller, A. Ellis, E. Muljadi, E. Camm, and B. Kirby, "Queuing up," *Power and Energy Magazine, IEEE*, vol. 5, pp. 47 –58, nov.-dec. 2007. 38

[87] J. Z. Z. Dr. Santoso, Dr. Muthumuni, "Distribution system analysis," June 21, 2006. 39

[88] `http://ewh.ieee.org/soc/pes/dsacom/testfeeders/index.html`. 39

[89] S. Santoso and Z. Zhou, "Induction machine test case for the 34-bus test feeder: a wind turbine time-domain model," in *Power Engineering Society General Meeting, 2006. IEEE*, p. 2 pp., 0-0 2006. 40

[90] P. Kundur, *Power System Stability and Control*. McGraw-Hill, Inc, 1994. 41

[91] "Dry-type power transformers," IEC standard - 60726 1982. 45, 46

[92] R. Harrold, "Acoustic waveguides for sensing and locating electrical discharges in high voltage power transformers and other apparatus," *Power Apparatus and Systems, IEEE Transactions on*, vol. PAS-98, pp. 449 –457, march 1979. 47

[93] Su, Ching-chau and Tang, Ya-wen and Tai, Cheng-chi and Chen, Jiann-fuh, "Detection and location of partial discharge in cast-resin dry-type transformers using a waveguide and a new acoustic emission sensor pair design," *Journal of Zhejiang University - Science C*, vol. 12, pp. 345–350, 2011. 10.1631/jzus.C1000126. 49

[94] *AC/DC Module User's Guide*, COMSOL 4.1 ed. 55, 57

[95] Y. Liu, "Finite element modeling of the frequency characteristic of transformers," Master's thesis, University of Toronto, 1996. 57, 59

[96] "IEEE Guide for Diagnostic Field Testing of Electric Power Apparatus - Part 1: Oil Filled Power Transformers, Regulators, and Reactors," *IEEE Std 62-1995*, pp. 0–1, 1995. 70

[97] Fuchs, E. F. and Kovacs, K. P. and Roesler, D. J., "Aging of Electrical Appliances Due to Harmonics of the Power System's Voltage," *Power Engineering Review, IEEE*, vol. PER-6, pp. 65 –66, july 1986. 72